TÉCNICO LISBOA

pH-Responsive Nanoparticles for Controlled Release

José Luís Martins Gonçalves

Thesis to obtain the Master of Science Degree in

Chemistry

Supervisors: Prof. Dr. José Paulo Sequeira Farinha

Prof. Dr. Carlos Miguel Calisto Baleizão

Examination Committee

Chairperson: Prof. Dr. Isabel Maria Delgado Jana Marrucho Ferreira

Supervisor: Prof. Dr. José Paulo Sequeira Farinha

Members of the Committee: Prof. Dr. Ana Clara Lopes Marques

June 2018

Resumo

Progressos recentes na área de Química dos materiais permitiram o desenvolvimento de dispositivos de resposta a estímulos, capazes não só de controlar temporal e espacialmente a entrega de um fármaco, mas também a dosagem a ser entregue. A utilização destes dispositivos requer o uso de materiais biocompatíveis suscetíveis a determinados estímulos físicos. As nanopartículas possuem este tipo de características e, por isso, têm atraído bastante atenção. Para além de melhorarem a farmacocinética de fármacos hidrofóbicos, solubilizando-os nos seus compartimentos hidrofóbicos, quando revestidas com polímeros que respondem a estímulos, as nanopartículas permitem controlar a entrega de fármacos em resposta a condições fisiológicas específicas. Adicionalmente, protegem as moléculas terapêuticas da metabolização fisiológica e aumentam a sua eficácia e bioavaliabilidade na corrente sanguínea, além de reduzirem os efeitos secundários. De entre uma grande variedade de nanomateriais inorgânicos, as nanopartículas de sílica mesoporosas (NSMs) têm características bastante atrativas para aplicação como sistema de veiculação de fármacos, devido às elevadas áreas superficiais, grande volume dos poros, elevada capacidade de carga, poros uniformes e ajustáveis e ainda, uma grande variedade de possibilidades de funcionalização da superfície.

O objetivo deste trabalho consistiu em preparar NSMs híbridas núcleo-coroa, revestidas com uma coroa polimérica de resposta ao estímulo de pH. Além disso, a incorporação de um pigmento fluorescente de elevado rendimento quântico na estrutura das NSMs permite combinar propriedades terapêuticas e de diagnóstico. A coroa polimérica foi preparada por polimerização RAFT (Reversible Addition-Fragmentation chain Transfer) de forma a obter uma coroa homogénea e bem-definida. As partículas híbridas obtidas têm um tamanho de cerca de 56 nm a valores de pH menores que 6.5.

O nosso sistema mostra que modulando o pH, é possível obter um regime de bombeamento que aumenta a velocidade de libertação de maneira controlada.

Palavras-chave: nanopartículas híbridas, nanopartículas de sílica mesoporosas, polimerização RAFT, resposta ao pH, coroa polimérica, libertação controlada

Abstract

Recent progress in material chemistry led to the possibility to develop stimuli-responsive devices that deliver a drug with spatial, temporal and dosage control. Implementation of such devices requires the use of biocompatible materials that are susceptible to specific physical stimuli. Nanoparticles have received much attention precisely because they comprise these characteristics. In addition to improving the pharmacokinetics of poorly soluble hydrophobic drugs, coated with stimuli-responsive polymers, nanoparticles allow the control of drug release in response to disease-specific physiological conditions. Additionally, they protect the therapeutic molecules from physiological metabolization and enhance its efficiency and bioavailability in the bloodstream, as well as reduce the side effects. Among a variety of inorganic-based nanomaterials, mesoporous silica particles (MSNs) have several attractive features for application as a drug delivery system due to their high surface areas, large pore volumes, high payload, uniform and tunable pore sizes, and a great diversity of surface functionalization options.

The goal of this work was to prepare core-shell MSNs, coated with a pH- responsive polymeric shell. In addition, by incorporating a high quantum yield fluorescent perylenediimide (PDI) dye in the MSNs pore structure, it is possible to combine diagnostic and therapeutic properties. Reversible Addition Fragmentation Chain Transfer (RAFT) polymerization was used to obtain a homogeneous polymeric shell with a well-defined structure. The hybrid nanoparticles have diameters around 56 nm at pH values lower than 6.5.

Our proof-of-concept system shows that by modulating the pH, it is possible to achieve a pumping regime that increases the release rate in a controlled way.

Key-Words: hybrid nanoparticles, mesoporous silica nanoparticles, RAFT, pH-response, polymeric shell, controlled release

General Contents

Figure Index

Scheme Index

Table Index

Abbreviation List

Abs	Absorbance
AIBN	2,2′-Azobis(2-methylpropionitrile)
APTES	(3-Aminopropyl) triethoxysilane
ATRP	Atom Transfer Radical Polymerization
BSPA	3-(benzylsulfanylthiocarbonylsulfanyl) propionic acid
CMC	Critical Micellar Concentration
CP	Chain Polymerization
CPADB	4-Cyano-4-(phenylcarbonothioylthio)pentanoic acid
CRP	Controlled Radical Polymerization
CSIRO	Commonwealth Scientific and Industrial Research Organisation
CTA	Chain Transfer Agent
CTAB	Hexadecyltrimethylammonium Bromide
D_H	Hydrodynamic Diameter
DDS	Drug Delivery System
DI	Deionized
DLS	Dynamic Light Scattering
DPA	2-(diisopropylamino)ethyl methacrylate
D_{TEM}	Diameter obtained by Transmission Electronic Microscopy
EDC	N-(3-dimethylaminopropyl) -N′-ethylcarbodiimide
EPR	Enhanced Permeation and Retention effect
GPC-MALS	Gel Permeation Chromatography Multi Angle Light Scattering
^{1}H NMR	Proton Nuclear Magnetic Resonance
IEP	Isoelectric Point
IS	Internal Standard
MCM-41	Mobil Composition of Matter Number 41
MSN	Mesoporous Silica Nanoparticles
MSN+APTES	Mesoporous Silica Nanoparticles Surface Modified with APTES
MSN+RAFT	MSN+APTES linked to RAFT Agent
MSN+PolyDPA	MSN coated with DPA polymer
NMP	Nitroxide-Mediated Polymerization
PolyDPA	Poly (2-(diisopropylamino)ethyl methacrylate)
PAA	Poly(acrylic acid)
PBS	Phosphate Buffered Saline

PDI	Perylenediimide
PEG	Polyethylene glycol
pKa	Acid Dissociation Constant
RAFT	Reversible Addition-Fragmentation Chain Transfer
RP	Radical Polymerization
TEM	Transmission Electronic Microscopy
TEOS	Tetraethyl Orthosilicate
TFA	TetraFluoroacetic Acid
SDA	Structure-Directing Agent
SEM	Scanning Electron Microscopy
SRB	Sulphorhodamine B
THF	Tetrahydrofuran
UV	Ultraviolet
UV-Vis	UV-Vis Spectroscopy

Unit List

℃	Degree Celsius
Da	Dalton
Eq	Equivalent
g; mg	Grams; milligrams (10^{-3} g)
h; min; s	hours; minutes; seconds
kV; mV	Kilovolts (10^{3} V); millivolts (10^{-3} V)
L; mL; µL	Litre; millilitre (10^{-3} L); microlitre (10^{-6} L)
M; mM	Molar; millimolar (10^{-3} M)
m, cm, µm, nm	meter; centimeter (10^{-2} m); micrometer (10^{-6} m); nanometer (10^{-9} m)
MHz	Megahertz
mol; mmol	Mol; millimol (10^{-3} mol)
rpm	Rotations per minute
x g	Times gravity

Symbol List

[APTES]	APTES concentration
[CTA]	CTA concentration
C	Concentration
Đ	Size Dispersity
$\mathbf{M_n^{GPC}}$	Number average molecular weight obtained by GPC-MALS
$\mathbf{M_n^{UV-Vis}}$	Number average molecular weight obtained by UV-Vis Spectroscopy
$\mathbf{M_n^{Target}}$	Target number average molecular weight
$\mathbf{M_w}$	Weight average molecular weight
M_w^{GPC}	Weight average molecular weight obtained by GPC-MALS
I_{IS}	Integrated intensity of the internal standard peak
$\mathbf{[CTA]_0}$	Initial CTA concentration
$\mathbf{[DPA]_0}$	Initial DPA Monomer concentration
ε	Molar Absorption Coefficient
[HCl]	HCl concentration
$\mathbf{[H_2SO_4]}$	H_2SO_4 concentration
[NaOH]	NaOH concentration
λ	Wavelength
$\boldsymbol{\lambda_{excitation}}$	Excitation Wavelength
$\boldsymbol{\lambda_{emission}}$	Emission Wavelength

1. Introduction

From ancient time, it has been the goal of the physician to provide patients with the best possible forms of medicines so that recovery from disease is faster and complete. The drugs are delivered in a suitable formulation, usually known as Drug Delivery System (DDS), keeping in view the safety, efficacy and system acceptability. These systems have been refined through the development of more reliable dosage forms such as tablets and capsules. During the last decades of the 20th century, a substantial effort was made to move from sustained, but essentially uncontrolled, release systems (e.g., waxes and other polymeric matrices) to controlled-release systems such as transdermal patches and improved oral-inhalation formulations. In the 1990s, the appearance of new drugs with larger molecular sizes, higher dose sensitivities, and often poorer stabilities in biological environments led to a stronger push towards the development of efficient encapsulation and controlled-release technologies. In addition to clinical efficacy and patient compliance, economic considerations (e.g., decrease in both frequency and cost of administering the drug) are driving the demand for versatile, high-performance controlled-release systems. (Barbø, Bartlett, and Kong 2007; Bharti and Gulati 2015; Blanco, Shen, and Ferrari 2015; Karimi, Ghasemi, and Sahandi Zangabad 2016)

From a technological perspective, controlled drug delivery implies the ability to control the distribution of therapeutic agents both in space and time. In other words, controlled drug delivery embodies both control of the rate of release of a drug, and the targeting. On one hand, controlled-release systems increase the overall efficacy of the drug by maintaining the drug concentration in the body within the optimum therapeutic range and under the toxicity threshold. On the other hand, the distribution of a drug between healthy and diseased cells can be overcome by selectively targeting the diseased sites. Successful targeting, requires the production of the DDSs in the form of nanoparticles (NPs) that can breach biological barriers to reach their specific target. The optimum particle size depends both on the route of administration and the targeted organ or cells, as well as the cargo itself. Desai *et al.* reported that 100 nm nanoparticles had a greater uptake than 1 µm and 10 µm microparticles in human colon cells. It has also been reported that the majority of cell lines incorporate 20 nm spheres containing DNA complexes, whereas for higher sizes the uptake becomes more specific and less effective. To cater for the various delivery options, a wide range of particulate-delivery systems (organic and inorganic) has been designed. (Barbø et al. 2007; Bharti and Gulati 2015; Blanco et al. 2015; Desai et al. 1997; Zauner, Farrow, and Haines 2001)

The blood stability represents a major problem for all organic delivery systems like liposomes and dendrimers. In the blood, protein markers (opsonins) adsorb on the surface of hydrophobic carriers, thus providing a signal to the immune system to evacuate these foreign entities from the body. Thus, to enhance circulation time in the bloodstream, the surface of the carrier needs to be functionalized with hydrophilic molecules, such as polyethylene glycol (PEG), in order to avoid detection by the immune system. This additional requirement disturbs the production process significantly, by requiring a total reformulation of the chemistry in the case of polymeric micelles

or increasing the manufacturing time of “stealth” liposomes to several days. (Barbø et al. 2007; Mohanraj and Chen 2006)

In contrast, metal oxide NPs have surfaces decorated with hydroxyl groups that render them intrinsically hydrophilic. This natural hydrophilicity should decrease oxide nanoparticle clearance, and thus increase their circulation time in the blood. The hydrodynamic stability in the blood stream is achieved by keeping the particle size between 50 and 300 nm. Above 300 nm, a significant proportion of the silica particles are trapped in the lungs and liver. Particles smaller than 50 nm can pass through small intercellular openings in the normal blood-vessel walls and thus tend to distribute non-specifically in the body. Metal oxides are also highly biocompatible, as demonstrated by their numerous applications as implants or coatings. In addition, the use of inorganic nanoparticles as DDSs require: (Barbø et al. 2007; Schulz and Mcdonagh 2012)

1. Easy manipulation of particle size and surface characteristics to achieve drug targeting after parenteral administration;
2. Controlled sustained release of the drug at a chosen localization, to achieve increase in drug therapeutic efficacy and reduction in side effects;
3. Easy modulation of the rate of release and particle degradation characteristics by choice of matrix constituents;
4. Site-specific targeting achieved by attaching targeting ligands to the surface of particles, or use magnetic guidance.

Silica nanoparticles, specifically, comprise these characteristics with a set of advantageous properties like robustness, mechanic strength, thermal and chemical stability, protection and stabilization of incorporated dyes, easy preparation and low size dispersity. (Barbø et al. 2007; Mohanraj and Chen 2006; Schulz and Mcdonagh 2012)

Mesoporous silica nanoparticles (MSNs) have attracted substantial attention due to their versatile structural properties, such as high specific surface area and large pore volume, colloidal stability, and the possibility to specifically functionalize the inner pore system and/or the external particle surface. These properties provide unique advantages to encapsulate a variety of therapeutic agents and deliver these agents to the desired location. Additionaly, the size, morphology, pore size, and pore strucuture of MSNs can be rationally designed accordingly to the desired application, using surfactants as structure-directing agents (SDAs). Therefore, by tailoring conditions such as the molar ratio of silica precursors and surfactants, pH control, and introduction of organoalkoxysilane precursors during the co-condensation reaction is possible to obtain particles with sphere-, rod-, to wormlike structures. Rapid progress has been achieved in the synthesis and application of ordered MSNs in catalysis, adsorption, separation, sensing, and drug delivery. (Argyo et al. 2013; Tang, Li, and Chen 2012)

1.1. Silica Nanoparticles

The various methods that have been used to obtain silica particles can be categorized into two main approaches: top-down and bottom-up (Figure 1). Top-down is a physical approach,

characterized by reducing the dimension of the original size by using special size reduction techniques. Bottom-up, in contrast, is a chemical approach which involves a common route used to produce silica nanoparticles from atomic or molecular scale. The bottom-up approach can produce much smaller sized particles and has the potential to be more cost-effective because of the advantages of obtaining a low dispersity, complete control over the process, and minimum energy loss compared with that of a top-down approach. Where the synthesis of nanoparticles is concerned, since precise control is required for achieving a uniform structure during the nanoparticle formation, the bottom-up approach has proven more suitable. (Chaudhuri and Paria 2012; Rahman and Padavettan 2012)

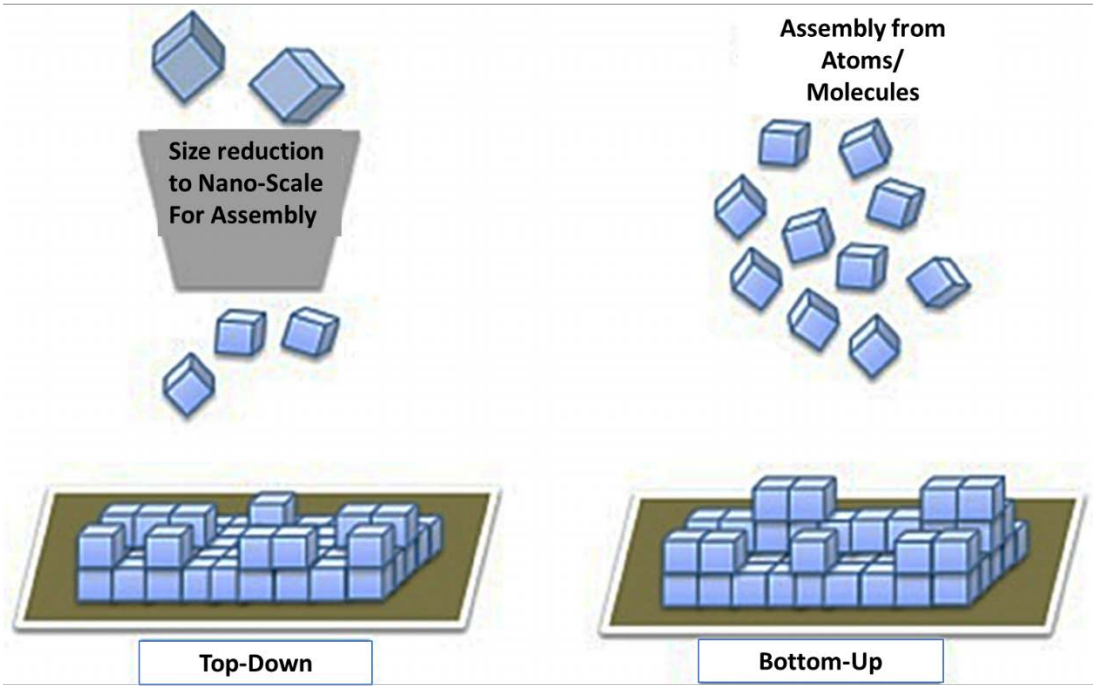

Figure 1 - Top down and bottom up approaches in nanotechnology. *(Barbhuiya and Qureshi 2014)*

1.1.1. Sol-gel method

The sol-gel process is one of the most common bottom-up approach and is widely used to produce pure silica particles due to its ability to control the particle size, size distribution and morphology through systematic monitoring of reaction parameters. It involves the development of networks through an arrangement of colloidal suspension (sol) and gelation to form a system in continuous liquid phase (gel). This method, depending on the nature of precursors, may be divided into two classes namely inorganic (chlorides, nitrates, sulphides, etc) and alkoxide precursors. In this process, the reaction of metal alkoxides and water (hydrolysis), in the presence of acid or base, forms one phase solution that goes through a solution-to-gel transition to form a rigid, two-phase system comprised of solid metal oxides and solvent filled pores. The physical and electrochemical properties of the resultant materials largely depend on the type of catalyst used. In the case of silica alkoxides, the acid catalysed reaction results in weakly cross-linked

linear polymers. Whereas, base-catalyzed reaction, due to rapid hydrolysis and of alkoxide silanes, forms highly branched clusters. This difference in cluster formation is due to the higher solubility of the silica oxide in basic medium. The reason is that high pH's favour the nucleophilic attack of the negatively charged silicates, increasing the condensation kinetic. (Chiang, Lian, and Leo 2011; Nakamura, Mizutani, and Nozaki 2007; Si-Han Wu 2013; Singh, Bhattacharyya, and Kumar 2014; Tang et al. 2012; Yano and Fukushima 2004)

Hydrolysis: $Si–(OR)_4 + H_2O \rightleftharpoons Si–(OR)_3(OH) + ROH$

Water Condensation: $(OR)_3–Si\text{-}OH + HO–Si–(OR)_3 \longrightarrow [(OR)_3Si–O–Si(OR)_3] + H–O–H$

Alcohol Condensation: $(OR)_3–Si\text{-}OR + HO–Si–(OR)_3 \longrightarrow [(OR)_3Si–O–Si(OR)_3] + R–O–H$

The complete hydrolysis to form $Si(OH)_4$ is very difficult to achieve. Instead, condensation occurs between either two –OH or Si–OH groups and an alkoxy group to form bridging oxygen and a water or alcohol molecules.

Successive condensation reactions lead to the formation of consecutive Si-O-SI bonds that interact cooperatively to form colloidal particles. With time the colloidal particles link together to form a three-dimensional network.

1.1.2. Stöber Method

In 1968, Stöber first discovered an effective method for the synthesis of monodispersed silica particles, which involves the hydrolysis of tetralkyl silicates in a mixture of alcohol and water using ammonia as a catalyst. (Si-Han Wu 2013; Stober 1968)

The diameter of silica particles from the Stöber process is controlled by the relative contribution from nucleation and growth processes. The hydrolysis and condensation reactions provide precursor species and the necessary supersaturation for the formation of particles. Ammonia works as a basic catalyst to this reaction (Figure 2). (Ibrahim, Zikry, and Sharaf 2010)

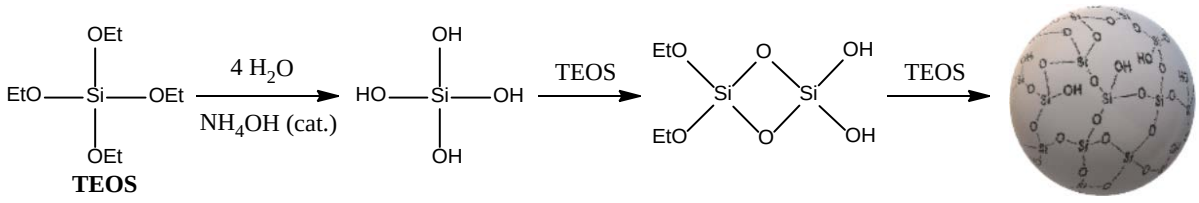

Figure 2 - Hydrolysis and Condensation Reactions of silica precursor TEOS.

The "Stöber Method" has been widely used, and subsequently particles with diameters ranging from tens of nanometers to a few microns have been obtained. With a careful control of the self-assembly and silica condensation kinetic, it is possible to tailor the sizes and morphologies, and if a SDA is used one can obtain mesoporous silica nanoparticles. (Si-Han Wu 2013)

1.1.3. Mesoporous Silica Nanoparticles Synthesis

The series of mesoporous materials, named Mobil Composition of Matter (MCM), first synthesized in 1992 by Mobil's researchers, have been keenly studied by researchers. MCM-41 and MCM-48 have attracted the most attention, due to their striking property of possessing a long range ordered framework with ordered mesopores, albeit being composed by amorphous silica wall. (Kresge et al. 1992)

With a surfactant such as cetyltrimethylammonium bromide (CTAB) as liquid crystal templating, tetraethyl orthosilicate (TEOS) or sodium metasilicate (Na_xSiO_x) as silica precursor, and a base as catalyst, MSNs with an ordered arrangement of uniform two-dimensional (2D) hexagonal mesopores were first synthesized and named as MCM-41. Surfactant self-assembly in aqueous solutions is a cooperative phenomenon and entropy driven process mainly governed by hydrophobic interaction. Since this process induce an order increase in the system, it is unfavourable from an entropic point of view. The driving force needed for amphiphilic molecules to spontaneously self-assemble into micelles and bilayers is usually denoted the hydrophobic effect. This force will only overcome the entropic dissociation force when the concentration of surfactant is above a certain value, which is called the critical micelle concentration (CMC). The shape of a surfactant molecule can be rationalized by its surfactant packing parameter. The packing parameter takes into account the volume of the hydrophobic chain the equilibrium area per molecule at the aggregate interface, and the length of the hydrophobic chain. (Bergström 2011; Kresge et al. 1992; Nagarajan 2002; Patel, Dharaiya, and Ray 2014; Tang et al. 2012)

The silica precursors condensate around the polar region of the micelles to form a silica structure around the surface of the micelles. After the reaction the template is removed by calcination or acid treatment (Figure 3). (Beck et al. 1992; Tang et al. 2012)

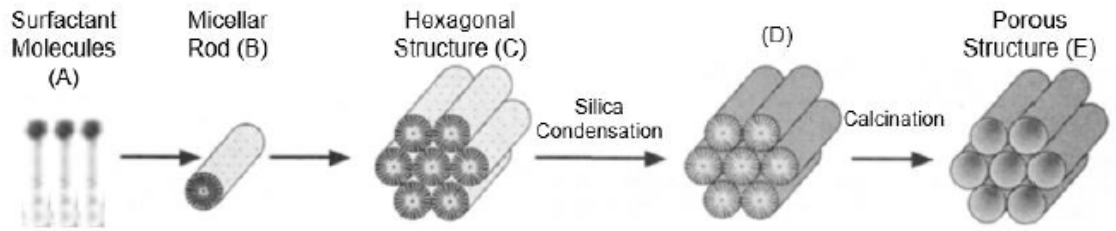

Figure 3 - Illustration of mesoporous material formation. [Adapted from Tang et al., 2012]

The material obtained by the classical procedure, however, yields particles with 1 µm or higher in size, with a wide size distribution. (Beck et al. 1992). It was reported that by modifying the Stöber synthetic compositions, spherical silica particles featuring an MCM-41 structure were obtained, instead of the hexagonal prisms obtained by other research groups. (Grün, Lauer, and Unger 1997) Since then, mixtures of alcohol, water and ammonia have been widely used with different template systems to prepare uniform MSNs with different pore sizes and mesostructures. The monodispersed MSNs are formed through the sudden aggregation of small clusters in the initial stage of the synthesis, followed by preferential reaction of the residual silica precursors with the

surface silanol on these existing particles. Indeed, the size of the MSN can be easily expanded by an additional silica source (such as TMOS) which reacts preferentially with the surface silanol groups on the existing particles rather than generating new particles by reacting with each other. This is the reason the Stöber-like process can generate uniform-sized MSNs. (Yano and Fukushima 2004) Finally, it is worth mentioning that the effects of the key reaction conditions (*e.g.*, amount of TEOS, pH value, and reaction time) on the resulting MSNs were investigated, and it was concluded that the pH value is the dominant parameter influencing particle size. This is due to the stability of the micelles in the reactional medium. At high pH values there will be more OH^- groups (after TEOS hydrolysis) to interact with the positive charges at the micelles surface, decreasing their stability. This charge screening induces the micelle aggregation, increasing the supramolecular aggregation number, and producing larger nanoparticles (Chiang et al. 2011)

1.2. Hybrid Nanoparticles

Nanoparticles can be categorized based on single or multiple materials into simple and core/shell or composite nanoparticles. As the name implies, composite and core/shell are composed of two or more materials. The core/shell type nanoparticles can be broadly defined as comprising a core (inner material) and a shell (outer layer material). These can consist of a wide of different combinations in close interaction, including hybrid nanoparticles, which combine organic and inorganic materials. (Chaudhuri and Paria 2012)

Hybrid nanoparticles composed of an inorganic core and a polymer shell have attracted great interest due to the intriguing properties associated with the nanocomposites. These types of particles have the dual properties of both the inorganic and organic materials. The inorganic shell, is beneficial in several aspects, such as increased strength of the overall material, resistance to oxidation, thermal and colloidal stability, and abrasion resistance. At the same time, these particles also show polymeric properties such as excellent optical properties, flexibility, and toughness, and in addition they can improve the brittleness of the inorganic. (Chaudhuri and Paria 2012; Hong, Li, and Pan 2007; Sailor and Park 2012)

The physicochemical properties of the nanoparticles such as size, surface charge and hydrophobicity/hydrophilicity play an important role in affecting their uptake by the phagocytic cell. It is generally accepted that nanoparticles with neutral and hydrophilic surface will have a longer blood circulation half-life. As such, the coating of the nanoparticles with a hydrophilic polymer (e.g. stealth coating) is the most commonly used method to modify the nanoparticle surface properties. However, nanoparticles composed by silica-polymer core-shell are hard to obtain, due to the incompatibility between inorganic-organic materials. Therefore, the synthesis of these NPs is assisted by functionalization of silica surface, leading to an increased compatibility between the two phases. (Amoozgar and Yeo 2012; Neoh and Kang 2011)

Undoubtedly, stealth polymer coatings can be designed to serve as a multifunctional platform, acting in synergy with the nanoparticles to provide new opportunities for therapeutic and diagnostic applications.

1.2.1 Surface Modification

The bioformulation with mesoporous materials as a theranostic system is promising due to the presence of free silanol groups on the surface that allows the incorporation of other groups from functionalized alkoxysilanes. The appropriate procedures of mesoporous material modifications enable an optimization of the drug adsorption and release. (Baeza, Colilla, and Vallet-Regí 2015)

The surface functionalization of these materials is also an important tool for the employment in different areas. The appropriate functional groups must be provided at the silica surfaces to enable specific interactions with the molecules needed in different applications (Figure 4). There are many reasons as to why functionalisation is important, but is mainly carried out to increase the loading of the molecules and to improve the interparticle and molecular relationships such as increasing the stability of the inorganic-organic bond and improving biocompatibility. (Baeza et al. 2015; Popat, Hartono, and Stahr 2011)

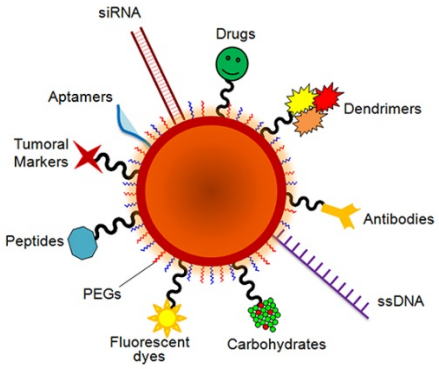

Figure 4 - Schematic illustration of silica nanoparticles' surface functionalization with various functional groups and (bio)molecules. *(Conde et al. 2014)*

As mentioned, the most popular way of covalently functionaled MSNs is by grafting the nanoparticles postsynthesis with the desired alkoxysilanes. This reaction is performed on mesoporous silica in nonpolar anhydrous solvents to avoid a reaction of the organosilanes with anything but the silica material. The reaction takes place between the silanol groups of the silica and the organoalkoxysilanes. The hydrolysable group (OR') reacts with the silanol groups located on the nanoparticle surface, anchoring the molecule covalently to the MSN surface (Figure 5) (Trewyn and Chen 2007)

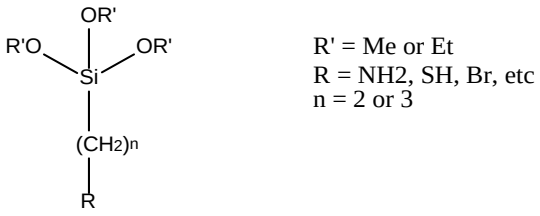

Figure 5 - Generic structure of a molecule anchored on the MSN surface.

The R group (figure 5) brings new physicochemical properties to the MSN surface, providing it with new functionalities. The grafting approach provides MSN with different regions of functionalization. The external surface as well as the pore entrance can be functionalized, while the surfactant is inside the pores avoiding internal functionalization. After the external surface functionalization, the surfactant can be removed, making the pores available to host molecules or to internal functionalization. (Trewyn and Chen 2007)

Recent studies on the interaction between surface-functionalized inorganic nanoparticles and animal cells have shown great potential for using these size-defined nanomaterials for various biomedical and biotechnological applications, such as cell type recognition and intracellular imaging. It has been shown that MSNs can be efficiently endocytosed by mammalian cells. The large surface areas and pore volumes of these materials offer the possibility of encapsulating and delivering large quantities of biogenic molecules through different cell membranes and to various intracellular targets. (Slowing, Trewyn, and Lin 2006)

Amine-functionalization has been reported as leading to a significant increase on loading capacity of mesoporous drug host. An example of an amine modifying agent is 3-(Aminopropyl) triethoxysilane (APTES), allowing the amino group to cover MSNs surface. This allows the subsequent drug loading or further addition of other organic molecules, such as polymers. (Ahmadi et al. 2014; Manzano, Aina, and Areán 2008)

1.2.2 Control-Radical Polymerization

Polymer grafting methods provide a very versatile tool to tailor the surface of nanoparticles and thus the interfaces between nanoparticles and the matrix polymers. These methods, when used with controlled radical polymerization (CRP), provide control over the type of polymeric architecture and composition to be grafted onto the particle surface, surface densities, and chain lengths at the nanometer scale. The methodologies to covalently graft polymer chains onto particles can be categorized into “grafting from” and “grafting to” (Figure 6). The “grafting to” method involves reacting the polymer chain previously prepared, bearing an appropriate functional group, to the particles surface. The random conformation of the chains “hides” its reactive region, leading to a slow kinetic. Furthermore, because of the steric hindrance imposed by the already grafted chains, it becomes increasingly difficult for the incoming polymer chains to diffuse to the surface against the concentration gradient of the existing grafted polymers, which intrinsically results in low graft densities. In contrast, the “grafting from” technique uses initiators that have been anchored to the particle surface, followed by the polymerization from the surface.

Since the existing grafted polymers will not hinder the diffusion of the small-sized monomers, significantly higher graft densities can be achieved with this technique. Nonetheless, it is important to mention that the molecular weight and the chain length distributions of polymer chains formed by the "grafting from" method cannot always be accurately controlled and measured. (Bhat et al. 2006; Hong et al. 2007; Li and Benicewicz 2005)

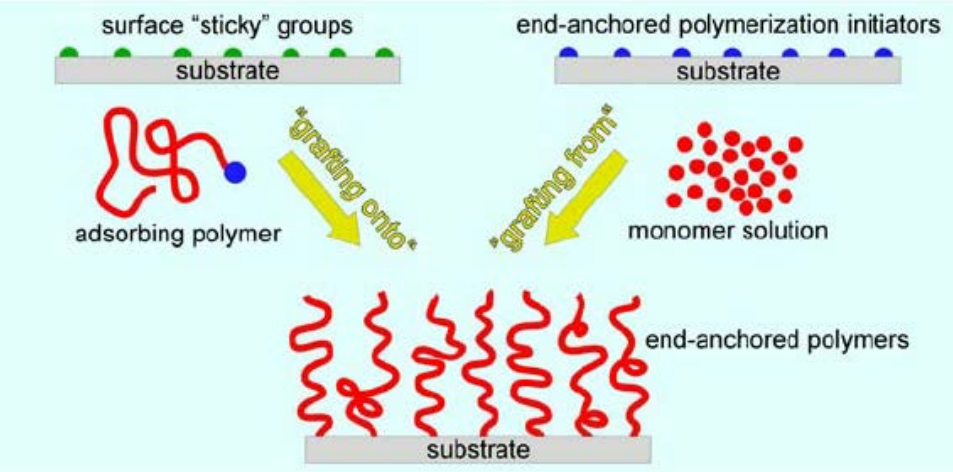

Figure 6 - Schematic illustrating the formation of surface-anchored polymer assemblies by utilizing the "grafting onto" and "grafting from" methods. *(Bhat et al. 2006)*

Reversible addition-fragmentation chain transfer (RAFT) has emerged as promising CRP technique due to its versatility and simplicity, and the polymer is free from the contamination of metal catalyst as in Atom Transfer Radical Polymerization (ATRP). (Hong et al. 2007; Hu et al. 2007)

RAFT polymerization is a smart reply to the drawbacks of conventional free radical polymerization, allowing control of the molecular weight distribution and the chain architecture, which allows to coat the nanoparticle external surface with a homogeneous shell. Whereas the other main CRP techniques are based on a reversible termination mechanism, i.e., ATRP (atom transfer radical polymerization), RAFT process is based on an identical reversible transfer mechanism. (Favier and Charreyre 2006; Hong et al. 2007; Hu et al. 2007)

In an ideal living polymerization, all chains are initiated at the beginning of the reaction, grow at a similar rate, and survive the polymerization: there is no irreversible chain transfer or termination. In reversible deactivation radical polymerization (RDRP), such as RAFT polymerization, the ideal conditions can be mimicked in the presence of chain transfer agents (CTAs) (figure 7), that induce reversible addition-fragmentation transfer reactions. CTAs can create an equilibrium between active species (propagating radicals) and so-called dormant species (thiocarbonylthio-terminated chains) that can become active again, contrary to the dead species. In other words, the RAFT agent controls and directs the polymerization, allowing the chains to grow at the same rate. Under these conditions, molecular weights can increase linearly with conversion and weight distributions can be very narrow and the majority of the polymerization product should be comprised of

dormant chains. (Chiefari et al. 1998; Favier and Charreyre 2006; Moad, Rizzardo, and Thang 2009)

The effectiveness of the RAFT agent depends on the monomer and is determined by the properties of the free radical leaving group R and the Z group, which can be chosen to activate or deactivate the thiocarbonyl double bond of the RAFT agent and modify the stability of the intermediate radicals (Figure 7).

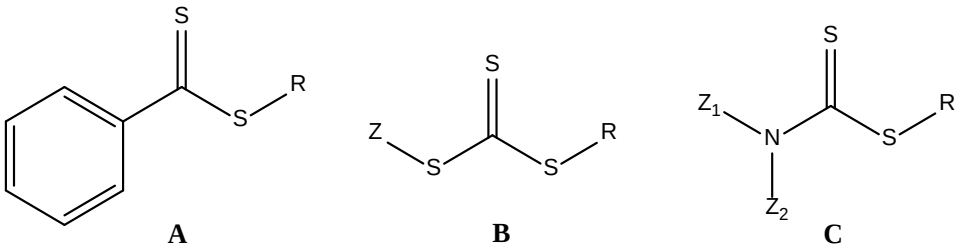

Figure 7 - Main class of RAFT agents: (A) dithiobenzoates;(B) Trithiocarbonates; (C) dithiocarbamates.

The mechanism of addition-fragmentation is based on the reaction between a propagating radical and a chain transfer agent, which bears both an activated double bond and a weak bond (Figure 8). Addition of the propagating radical to the unsaturation induces the formation of an intermediate radical (IR) which undergoes a fragmentation reaction that involves the weak bond. The released radical enters the polymerization cycle.(Favier and Charreyre 2006; Moad et al. 2009)

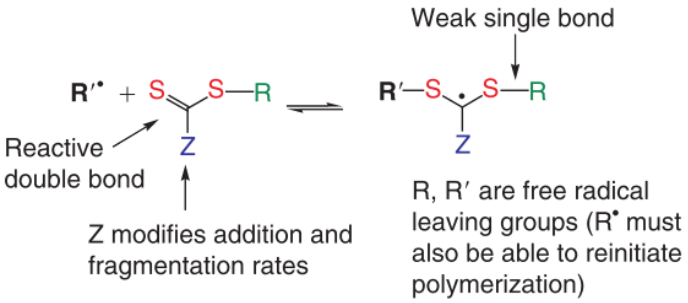

Figure 8 - Structural features of thiocarbonylthio RAFT agent and the intermediate formed on radical addition. *(Moad et al. 2009)*

The commonly accepted mechanism of the RAFT polymerization is as described in Scheme 1. Initiation and radical-radical termination occur as in conventional radical polymerization. In the early stages of the polymerization, addition of a propagating radical (P_n^*) to the thiocarbonylthio compound followed by fragmentation of the intermediate radical provides a polymeric thiocarbonylthio compound and a new radical (R^*). Reaction of this radical with monomer forms a new propagating radical (P_m^*). Rapid equilibrium between the active propagating radicals and the dormant polymeric thiocarbonylthio compounds provides equal probability for all chains to grow and allows to produce narrow dispersity polymers. When the polymerization is complete (or stopped), most of the chains (with exception to those initiate by the initiator) retain the thiocarbonylthio end-group and can be isolated as stable materials. The reactions associated with

RAFT equilibria are in addition to those (i.e., initiation, propagation, transfer, and termination) that occur during conventional radical polymerization. (Chiefari et al. 1998; Moad et al. 2009)

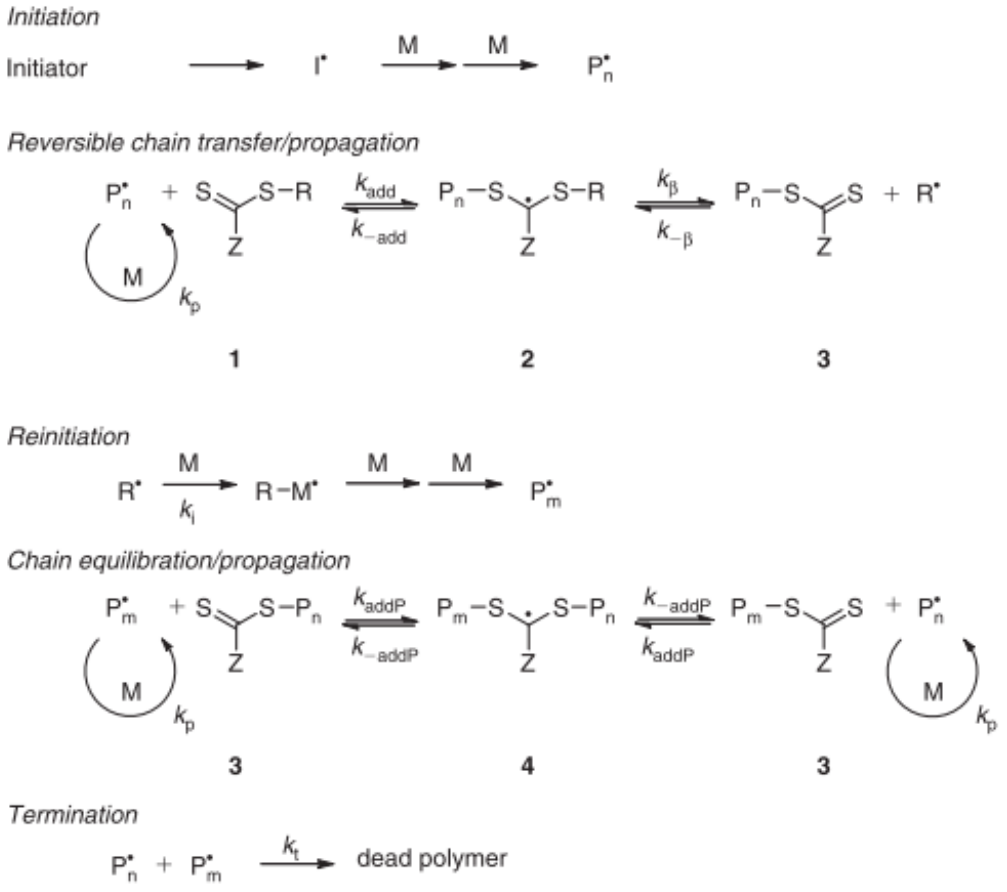

Scheme 1 - Mechanism of RAFT polymerization. (Moad et al. 2009)

Like in a conventional free-radical polymerization, the active species can also propagate and terminate. However, in a RAFT polymerization, the amount of initiator, and thus the concentration of active species, is lower and the termination reactions are minimized. (Favier and Charreyre 2006)

In order to obtain an efficient RAFT polymerization, several requirements must be fulfilled: fast and quantitative initiation of the polymer chains, thus the RAFT agent should have a high transfer constant; both the addition and fragmentation rate should be high and of comparable magnitude in order to limit the number and the lifetime of intermediate radicals; the number of monomer units added every time that the chain is active should be low. Therefore, the transfer rate of the active species with RAFT agent should be similar or higher than the propagation rate; and the occurrence of any reaction that leads to the formation of dead chains should be minimized, therefore, any side reaction with thiocarbonylthio function of the dormant species should be avoided, and the active species concentration should be as low as possible while keeping a

satisfactory polymerization rate (high $[\text{RAFT agent}]_0$/ $[\text{initiator}]_0$ ratio). (Chiefari et al. 1998; Favier and Charreyre 2006)

RAFT polymerization is of great interest due to the possibility of anchoring the CTA onto nanoparticle surface. This allows to obtain hybrid nanoparticles with a polymeric shell grown from the core ("grafting from" method), with a controlled "thickness". (Moad et al. 2009)

1.3. Stimuli-responsive Controlled Delivery Systems

The development of stimuli-responsive nanomaterials has been receiving extensive attention in recent years and now has become a principal field in medical research. (Baleizão and Farinha 2015)

By decorating hybrid MSNs with appropriate groups, the efficacy of the drugs can be enhanced since nonspecific toxicity is reduced and the local dose delivered to the chosen location can be higher. (Baleizão and Farinha 2015; Chang, Chen, and Wang 2013)

Various types of nanoparticles, organic molecules, and biomolecules, have been used as agents to block molecule transport from a silica mesopore and to unlock the entrance for release under specific external stimuli. (Cayre and Biggs 2011)

One reliable strategy is to build environment-responsive polymer-coated MSN systems a combination that creates a novel type of control-release nanocarrier that takes advantage of the unique features of polymers and porous materials. (Cayre and Biggs 2011; Chang et al. 2013; Karimi et al. 2016; Liu et al. 2011; Xing et al. 2012)

The current large interest in responsive polymers has arisen due to their ability to undergo reversible conformational changes in solution (solubility, conformation in solvent, etc) as a function of the external environment. Indeed, responsive polymers can adapt their behaviour in solution in response to a range of stimuli such as temperature, pH, ionic strength, light, biological conditions or mechanical stress. (Cayre and Biggs 2011; Chang et al. 2013)

In Figure 9 is represented the case of a pH-responsive polymer, specifically a polybase. At pH values lower than its pKa, the polymer is positively charged and expands due to the electrostatic repulsion interacting with the water molecules. When the pH rises, it loses its ionic character and collapses.

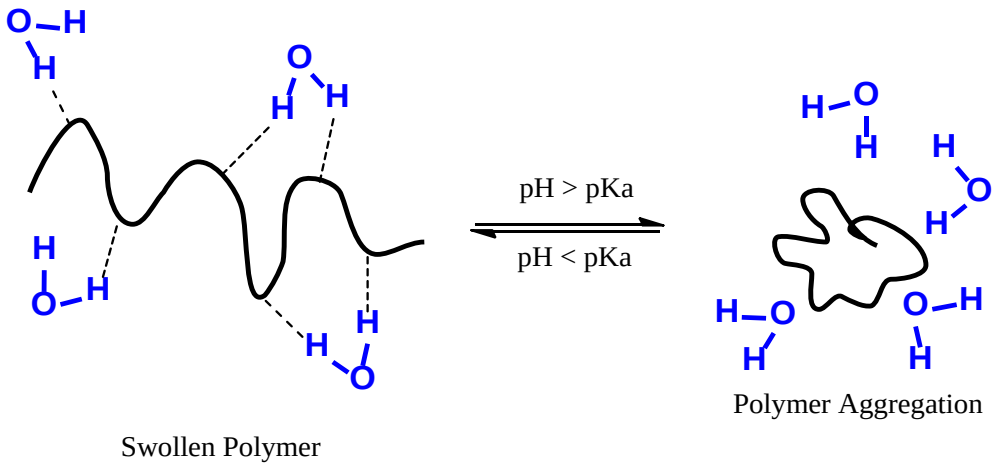

Figure 9 - Schematic representation of responsive polymer responding to change in pH. Adapted from (Shakya et al. 2010)

For drug release, pH and temperature are the most used stimuli. Temperature is called an external stimulus since it must be changed by an external source. pH, on the other hand, is called an internal stimulus since it changes within the body. Therefore, it can be used to produce a response of the system in a certain tissue or cellular compartment without any external help. This makes pH-responsive polymers a more attractive option to be used in controlled drug systems. (Gao, Chan, and Farokhzad 2010)

It is noteworthy that the pH changes along the gastrointestinal tract, from acidic in the stomach to basic in the intestine, must be considered in oral delivery. However, there are subtle changes within different tissues that make pH-responsive delivery an effective strategy. For example, chronic wounds have been reported to have pH values between 7.4 and 5.4 and most cancer tissues have lower extracellular pH values (pH = 5.7-7.8) than the corresponding healthy tissues and the bloodstream. The acidity of tumour microenvironments is caused in part by lactic acid accumulation in rapidly growing tumour cells owing to their elevated rates of glucose uptake but reduced rates of oxidative phosphorylation. This persistence of high lactate production by tumours in the presence of oxygen, provides a growth advantage for tumour cells *in vivo*. These features can be used to create pH-sensitive MSN-based carriers that intelligently distinguish microenvironment difference between normal and tumour tissue, achieving a better targeting and treatment efficiency. (Cayre and Biggs 2011; Chang et al. 2013; Gao et al. 2010; Schmaljohann 2006)

A number of studies have reported the development of pH-responsive MSN nanocarriers through surface functionalization of MSN with various materials as gatekeepers. The triggered release of drugs from MSN nanopores was achieved mainly by using polyelectrolytes, supramolecular nanovalves, pH-sensitive linkers, and acid-decomposable inorganic materials. (Moreira, Dias, and Correia 2016)

There are very few works regarding the use of pH-responsive polymer shell as a nanovalve on the exterior surface of MSNs. The ones that do so, prepare the polymer shell using graft-from

strategies, by either free radical polymerization or Atom Transfer Radical Polymerization. In the first case, it is difficult to control the molecular weight of grafted polymers, in the second it is necessary to clean up the catalysts. Furthermore, the polymers used are restricted to PEG and Poly(acrylic acid) (PAA). (Hong, Li, and Pan 2009; Yuan, Tang, and Yang 2011)

1.4. Objective and Work Strategy

The aim of this work was to develop hybrid mesoporous silica nanoparticles with silica nanostructured core and a shell of pH-responsive polymer. The biocompatible polymer used is based on a polybase of a tertiary amine methacrylate monomer, 2-(diisopropylamino)ethyl methacrylate (DPA) (Figure 10). In addition, by incorporating a high quantum yield fluorescent perylenediimide (PDI) (Figure 11) dye in the MSNs pore structure, we were able to combine diagnostic and therapeutic properties. (Rodrigues et al. 2013; Santiago, Baleizão, and Farinha 2015)

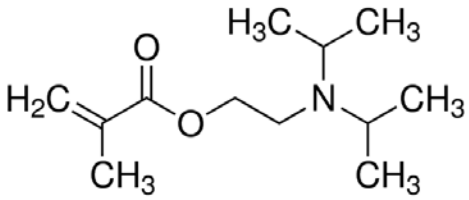

Figure 10 - Structure of DPA monomer.

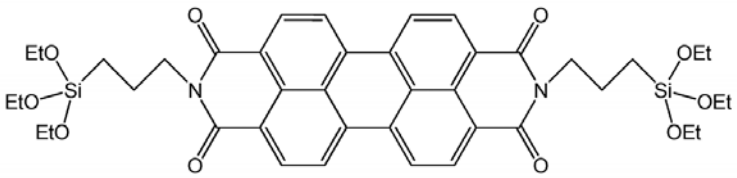

Figure 11 - Structure of PDI dye.

The fluorescent dye was adsorbed to the structure of the surfactant hexadecyltrimethylammonium bromide (CTAB). The MSNs were synthesized by the hydrolysis and condensation of tetraethoxysilane (TEOS) around the polar region of the CTAB micelles forming a silica structure around the surface of the micelles, obtaining fluorescent MSNs. Then, an amino surface modification was performed with (3-Aminopropyl) triethoxysilane (APTES), followed by surfactant removal, ensuring the availability of the porous for later molecule incorporation. (Santiago et al. 2015)

The silica precursors condensate around the polar region of the micelles to form a silica structure around the surface of the micelles.

After that, a CTA was covalently immobilized on the MSNs surface to initiate a controlled DPA monomer polymerization from the surface. This method, known as “grafting from”, was performed by anchoring the carboxylic group of the CTA to the amine group located on MSN surface. The

RAFT agent used was 4-Cyano-4-(phenylcarbonothioylthio)pentanoic acid (CPADB), and with this process is possible to obtain hybrid MSNs with high polymeric density, distribution and controlled thickness, obtaining MSN+PolyDPA.

In order to verify the efficiency of the RAFT agent and determine the kinetics and optimal conditions of the reaction, the polymerization was conducted in solution without nanoparticles. The polymer used for coating MSN, PolyDPA is highly biocompatible and pH sensitive, with pKa around 6.5. (Zhou, Wang, and Huang 2011)

This hybrid system is a good candidate as drug delivery system with interesting applications on cancer treatment. This type of systems can take advantage of the polymeric conformational transition since its occurs in the pH range of tumour cells. The mechanism expected for controlled drug release is illustrated in Scheme 2. In a basic/neutral medium (pH > 6.5), the polymeric shell exhibits hydrophobic behaviour due to its deprotonation, allowing a collapsed (unswollen) conformation that protects the drug loaded inside the MSN pores from diffusion. On the other hand, when the medium becomes acidic (pH < 6.5), the polymer protonates turning into a cationic soluble polyelectrolyte due to the protonation of its amine, showing an extended (swollen) conformation, that allows a gradual diffusion of the drug molecule into the medium.

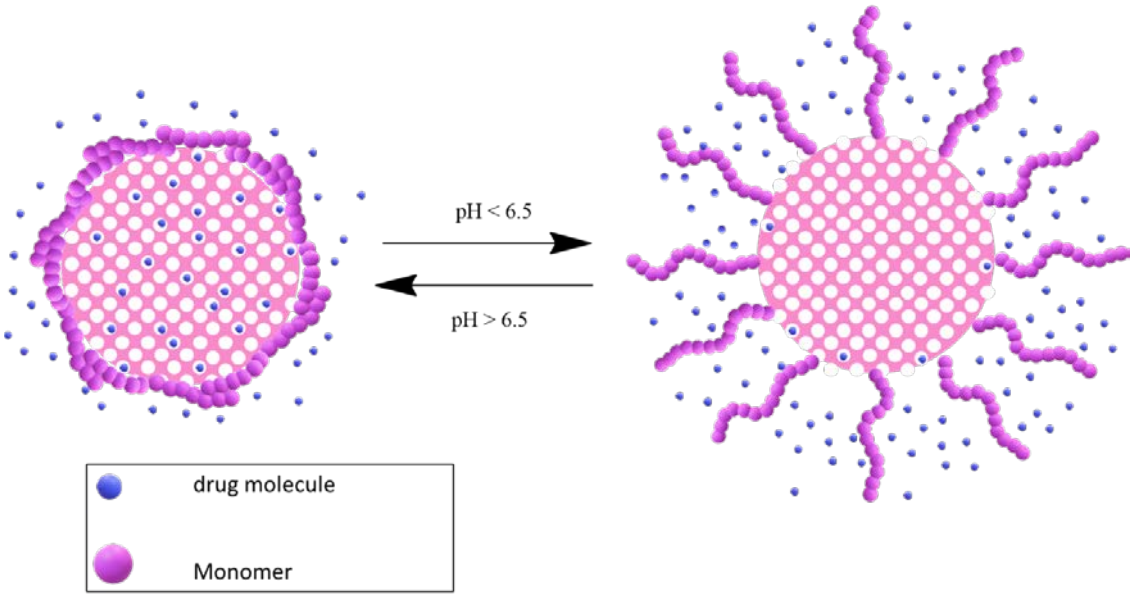

Scheme 2 - Schematic illustration of controlled drug release by MSN+PolyDPA.

2. Experimental Section

2.1. Materials

Absolute Ethanol (99.9 % EtOH, Scharlau, Barcelona, Spain), hexadecyltrimethylammonium bromide (99 % CTAB, Sigma, St. Louis, MO, USA), sodium hydroxide (Pure NaOH, EKA Pellets, Bohus, Sweden) and tetraethoxysilane (99 % TEOS, Aldrich, St. Louis, MO, USA) were all used as received for synthesis of mesoporous silica nanoparticles (MSNs). The deionized (DI) water was generated using a Millipore Milli-Q system (≥18 MΩcm, Merck, NJ, USA). The dye incorporated into MSNs, PDI derivative, was synthesized according to the literature. (Santiago et al. 2015)

(3-Aminopropyl) triethoxysilane (98 % APTES, Sigma-Aldrich), without any treatment, was used for surface modification in dry toluene which was distilled over calcium hydride before use. The surfactant templates were removed using a 0.5 M hydrochloric acid solution (37 % HCl, AnalaR NORMAPUR - VWR, Radnor, Pennsylvania) in absolute EtOH.

For chain transfer agent (CTA) immobilization, N-(3-dimethylaminopropyl) -N′-ethylcarbodiimide (98 % EDC, Sigma-Aldrich) in dry dichloromethane and 3-(benzylsulfanylthiocarbonylsulfanyl) propionic acid (BSPA) or 4-Cyano-4-(phenylcarbonothioylthio)pentanoic acid (CPADB, 97 %, Sigma-Aldrich) as CTA, were used. (Stenzel, Davis, and Fane 2003)

In order to synthesize the monomer 2–(diisopropylamino) ethyl methacrylate (DPA), hydroquinone (99 %, Aldrich Chemistry), methacryloyl chloride (97 %, Aldrich), and 2–(diisopropylamino) ethanol (98 %, Aldrich Chemistry) were all used as received. Over time, it was necessary to distil 2-(diisopropylamino) ethanol in vacuum, due to degradation of the amine. Also, tetrahydrofuran (99 % THF, Aldrich) dried with sodium and dry triethylamine distilled over calcium hydride were used.

For the RAFT polymerization of 2–(diisopropylamino) ethyl methacrylate, tetrahydrofuran (99.9 % THF, Aldrich), azobisisobutyronitrile (AIBN, 99 %, Sigma-Aldrich) recrystallized, Trifluoroacetic acid (>99 %, Merck), absolute EtOH and 1,4 - Dioxane previously dried with sodium and distilled were used.

Sodium dihydrogen phosphate monohydrate (NaH_2PO_4, 98%, Panreac), disodium hydrogen phosphate (Na_2HPO_4, 99%, Riedel-de-Haen) and sodium hydroxide (NaOH, 98%, Sigma-Aldrich) were used to prepare the phosphate buffer solutions (PBS, 100 mM pH 5 and pH 9). Sulforhodamine B (SRB, Molecular Probes) was used as a model molecule for the release studies. Deionized water from a Millipore system Milli-Q ≥18 MΩ cm (with a Millipak membrane filter 0.22 µm) was used in the preparation of solutions and in synthesis.

For DLS and ζ-Potential measurement we used 3 mL plastic syringes (B-BRAUN, Germany), sodium dodecyl sulphate (98 % SDS, Aldrich) and cellulose 0.45 µm cellulose filters (VWR). Capillary cells (DTS1070) (Malvern Instruments, Worcestershire, UK) were used for ζ-Potential

measurements and disposable polystyrene cuvettes (Brand GMBH, Germany) for DLS measurement. TEM images were acquired by preparing well-dispersed MSNs and MSN+PolyDPA samples and placed in carbon grid (Ted Pella, USA) by using iTEM software.

Chloroform-D (99.8 %, Cambridge Isotope Laboratories, MA, USA) and deuterium oxide (D_2O 99.9 %, Cambridge Isotope Laboratories), supplemented with NaOH and 1,3,5-trioxane (99.0 %, Fluka, Germany), were used for quantitative and qualitative characterization by ^1H NMR. UV-Visible Spectroscopy was performed using MSN or polymer sample dispersion in quartz cuvettes (Hellma Analytics, Müllheim, Germany) with 1 cm x 1 cm dimension. The MSN samples were prepared with a concentration of 1.0 mg/mL in dioxane and the polymer samples were prepared with a concentration of 1.0 mg/mL in THF.

2.1.1. Equipment

Centrifuge

An Avanti J – 30I Centrifuge (Beckman Coulter, California, USA), rotor JA – 30.50 Ti, was used for cleaning MSNs. For the centrifugations, 50 mL centrifuge tubes from the same manufacturer were used. Centrifugal Refrigerator (3-16K) (Sigma Zentrifugen, Osterode am Harz Germany), rotor 12141, was used for washing functionalized MSNs. Disposable 10 mL polypropylene tubes were used for the centrifugations.

Transmission Electronic Microscopy (TEM)

TEM images were obtained on a Hitachi transmission electron microscope (Hitachi High – technologies, Tokyo, Japan), model H-8100, with a LaB_6 filament (Hitachi) complemented with an accelerator voltage of 200 kV. A camera KeenView (Soft Imaging System, Münster, Germany) is incorporated in this equipment, which through iTEM software, allows acquiring TEM images. MSN dispersed in ethanol were prepared and dried on a carbon grid. The size/dimension, polydispersity, and morphology of the particles were estimated by evaluating at least 50 nanoparticles by Image J software.

Scanning Electronic Microscopy (SEM)

SEM images were obtained on a JEOL SEM (model JSM7001F, JEOL, Tokyo, Japan), with an accelerating voltage of 15 kV. One drop of particle dispersion in ethanol was placed on the sample holder and dried in air. The SEM samples were coated with chromium using a turbo-pumped sputter coater from Quorum Technology (model Q150T ES, Quorum Technology, Ashford, UK) for 1 min. The size/dimension, polydispersity, and morphology of the particles were estimated by evaluating at least 50 nanoparticles by Image J software.

Dynamic Light Scattering (DLS) and ζ-potential

Zetasizer Nano ZS (Malvern Instruments, UK), model ZEN3600, with 173º and 90º detector was used in order to determine hydrodynamic particle radii in solution. The estimation of the nanoparticles size is based on the dynamic light scattering (DLS) assuming Brownian movement

of the nanoparticles. DLS yields quantitative measurement of the mobility of scattering particles in solution as characterized by their self-diffusion coefficient. This is possible because of the temporal changes in interparticle positions and the corresponding temporal concentration fluctuations, reflecting the Brownian motion of the scattering particles. Then, this is analyzed by an algorithm (CONTIN method, in the present work) and the self-diffusion is determined. Finally, using the Stokes-Einstein equations the nanoparticle's hydrodynamic diameter (D_H) is determined. The ζ-Potential was measured in every step, the surfactant being previously removed, by dispersing 1 mg of particles in 1 mL of Milli-Q water (pH≈5).

^{1}H NMR

Proton Nuclear Magnetic Resonance (^{1}H NMR) (δH) spectra were recorded on an AMX-400 instrument (Bruker, MA, USA). For this purpose, two solutions of NaOH and 1,3,5-trioxane (internal standard, IS) in D_2O were prepared. In order to assess and quantify the quantity of APTES immobilized, ^{1}H NMR was performed. In a NMR tube, 0.5 mg of particles, 400 µL of a solution of NaOH and 100 µL of a solution of 1,3,5-trioxane were mixed and sonicated, until a clear solution was obtained.

UV-Vis Spectroscopy

UV-660 UV-VIS Spectrophotometer (JASCO International, Tokyo, Japan), supplied with a double monochromator and a photomultiplier detector for higher resolution, was employed for UV-Vis spectroscopy assays.

GPC

Polymer shells and polymer samples were characterized by GPC-MALS in THF using a Waters 510 pump fitted with three columns (Phenolgel™ from Phenomenex, Torrance, CA, USA, with pore size 100, 1,000, and 10,000 Å; column temperature: 296.15 K) connected in series and a miniDAWN-treos multiangle laser light scattering detector from Wyatt Technologies (Santa Barbara, CA, USA) and a Waters 2410 refractive index detector at 303.15 K. This is a type of size exclusion chromatography, that separates based on the size or radius of gyration of the analytes. This differs from other separation techniques which depend upon chemical or physical interactions to separate analytes. Separation occurs via the use of porous beads packed in a column.

pH

The pH of the solutions for the release study was measured with a bench pH/mV/°C meter pH 1000L, pHenomenal®.

Fluorescence

Fluorescence measurements were obtained on a Horiba-JobinYvon Fluorolog-3 spectrofluorimeter using a fluorescent cell. Right angle geometry was used in all measurements.

For the release study a polypropylene dialysis device with a cellulose membrane (Slide-A-Lyzer Mini DialysisDevices, 10K MWCO) was used.

2.2. Methods

2.2.1. Synthesis of Fluorescent Mesoporous Silica Nanoparticles

MSNs were synthesized by a modified sol-gel process. In a 15 mL polypropylene flask, CTAB (0.5 g) and PDI (1.6 mg) were mixed in THF (5 mL). The mixture was sonicated in order to dissolve the PDI and was left stirring at 40 ℃ until THF was evaporated (approximately 24 h). In a 500 mL polypropylene flask, deionized (DI) water (240 mL) and a NaOH solution (1 M or 1.7 M, 1.75 mL) were added. After the temperature inside the flask was stabilized at 32 ℃, the solid mixture CTAB/PDI was added. After 30 min, TEOS (2.5 mL) was added dropwise, and the solution was left stirring for 3 h. The MSNs were recovered by centrifugation at 30,000 × g for 20 min at 20 ℃ and washed twice with a mixture of ethanol and water (50% v/v) and once with absolute ethanol, discarding each time the supernatant. Alternatively, MSNs were recovered by filtration under vacuum. The solid product obtained was dried at 50 ℃ overnight. Finally, the particles were dried under vacuum.

2.2.2. Modification of Mesoporous Silica Nanoparticles Surface

Amino modification of the silica was performed by suspending the obtained nanoparticles in dry toluene (18 mL per 500 mg of nanoparticles) and sonicating it for 15 min, under argon atmosphere. Afterwards, APTES (0.15 mL) was added dropwise and the resulting mixture was put under reflux (T= 130 ℃) for 24h under argon atmosphere. The solid product (MSN+APTES+CTAB) was obtained by centrifugation at 13081 rpm for 10 min at 18 ℃., and washed three times with absolute ethanol, discarding each time the supernatant. The particles were dried in a ventilated oven for 24 h at 50 ℃.

An acidic ethanol solution ([HCl] = 0.5 M, 25 mL per 500 mg of MSN) was used to remove the template, by re-suspending MSN+APTES+CTAB and sonicating it for 15 min. Subsequently, it was left under stirring at 50 ℃ for 24 h. MSN+APTES were recovered by centrifugation at 13081 rpm for 10 min at 18 ℃ and washed once with a basic ethanol solution (NH_4 25%v/v) and five times with absolute ethanol, until until neutralization of the supernatant. The product was dried at 50 ℃ under vacuum for 24h. (Scheme 3)

^{1}H NMR (D_2O): 0.38 ppm (t, 2H, Si-CH_2-); 1.41 ppm (q, 2H, -CH_2-); 2.49 ppm (t, 2H, -NH_2); 1.09 ppm (solvent, C**H**$_3$$CH_2OH$); 3.57 ppm (solvent, CH_3C**H**$_2$OH); 4.71 ppm (D_2O); 5.15 ppm (internal standard, C_3**H**$_6$$O_3$)

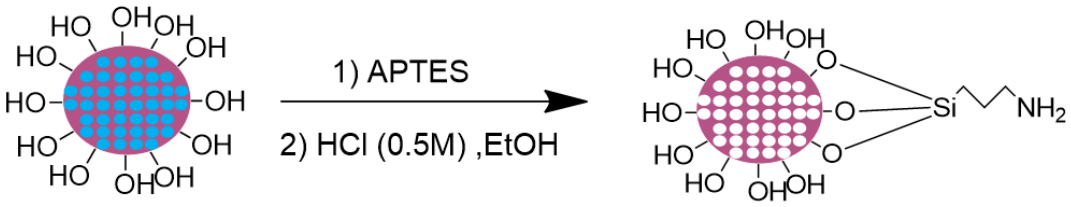

Scheme 3 - APTES surface modification scheme.

2.2.3. Immobilization of Chain Transfer Agent

In order to immobilize CTA on the nanoparticles' surface 15 mL of dry dichloromethane was added per 250 mg of MSN+APTES into a 25 mL flask under argon atmosphere and sonicated for 20 minutes. Then, 3-(benzylsulfanylthiocarbonylsulfanyl) propionic acid (BSPA) or 4-Cyano-4-(phenylcarbonothioylthio)pentanoic acid (CPADB) (1 eq to APTES) was added to the mixture, at low temperature. After 10 min, EDC (1.2 eq to APTES) was added and the mixture was left stirring, under argon atmosphere, at room temperature for 24h. MSN+CTA were recovered by centrifugation at 12000 rpm for 10 min at 18 ℃., and washed three times with absolute ethanol, discarding each time the supernatant. (Scheme 4)

UV-Vis: BSPA: $\lambda_{Máx}$ = 310nm; CPADB: $\lambda_{Máx}$ = 304 nm

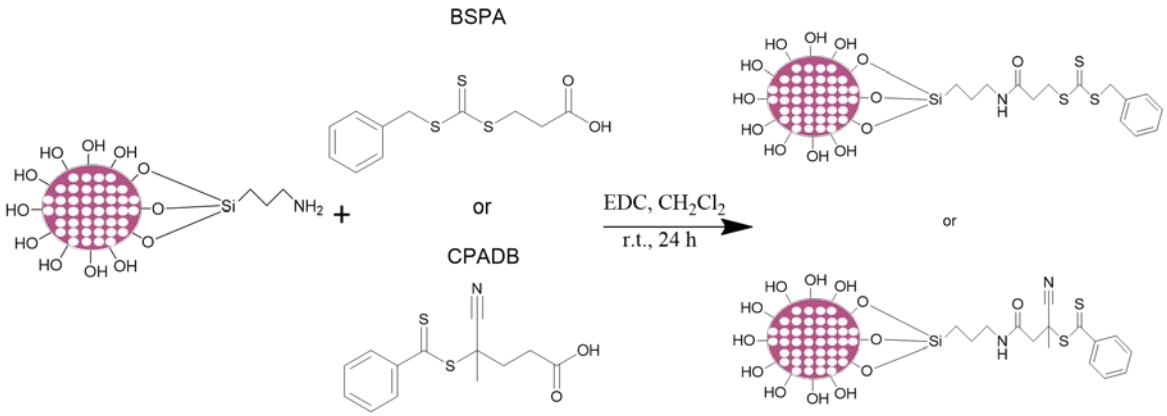

Scheme 4 - CTA Immobilization scheme on MSN surface.

2.2.4. Synthesis of 2–(diisopropylamino) ethyl methacrylate (DPA) Monomer

The monomer 2 – (Diisopropylamino) ethyl methacrylate (DPA) was obtained through the acylation of a primary alcohol with a methacriloyl, with a moderate yield (65-70%).

To a solution of hydroquinone (40 mL) in dry THF (40 mL) under argon atmosphere was added dry triethylamine (4 mL, 1 eq) and 2-(diisopropylamino ethanol) ethanol (4.8 mL, 1 eq) and stirred on ice. Afterwards, methacryloyl chloride (2.8 mL, 1 eq) was added dropwise for 15 min, and the mixture was left under reflux for 2 h. The reaction was filtered, and the solvent was evaporated until a yellow oil was obtained. Lastly, the "yellowish" oil was distilled under reduced pressure at 130 ℃, and a transparent oil was obtained.

The synthesis was confirmed by ^{1}H NMR. In figure 12 it is shown the ^{1}H NMR spectra of the synthesized DPA.

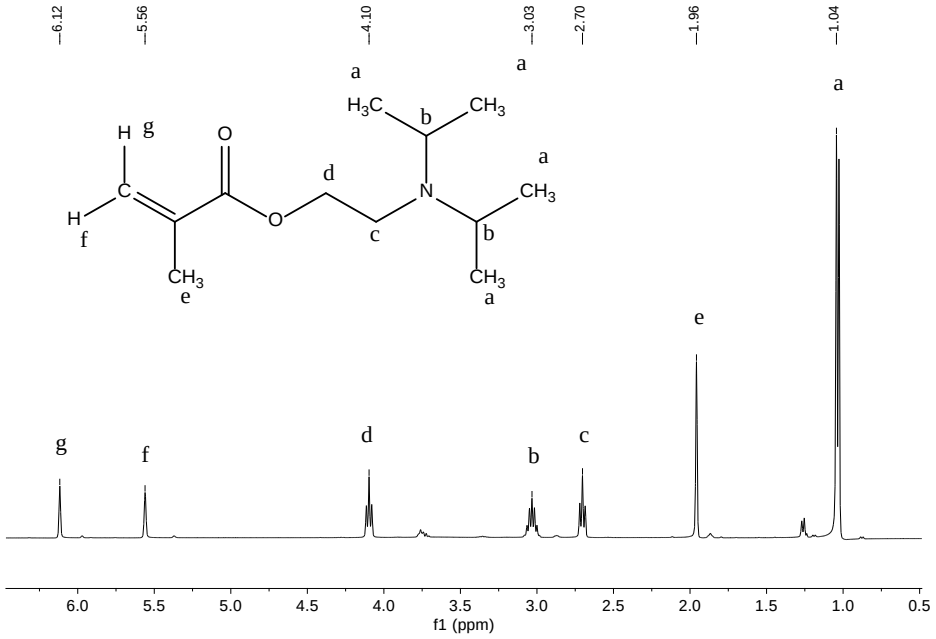

Figure 12 - ^{1}H NMR Spectra of Monomer DPA in $CDCl_3$.

^{1}H NMR ($CDCl_3$): 1.04 ppm (d, 12H, -CH-C**H**$_3$); 1.96 ppm (s, 3H, -C=C-CH_3); 2.70ppm (t, 2H; -CH_2-N); 3.03 ppm (m, 2H, -N-CH-); 4.10 ppm (t, 2H, -O-CH_2-); 5.56 ppm (s, 1H, CH_2=C-); 6.12 ppm (s, 1H, CH_2=C-, affected by the oxygen electron cloud from the ester group).

2.2.5. Kinetics of RAFT polymerization

Route 1

In a Schlenk tube 8.2 mg of BSPA were added under vacuum. Afterwards, under argon atmosphere, 1,4-dioxane (0.5 mL), DPA (0.33 mL, 1 eq) and a solution of AIBN in 1,4-dioxane ([AIBN] = 1mg/mL, 0.5 mL)) were added. The molar ratio of AIBN and CTA was kept constant (1:10). Atmosphere oxygen was removed by bubbling the solution with argon for 1 h. Finally, the mixture was put in a bath at the desired temperature (70 ℃, 80 ℃ or 90 ℃) for 24h. Samples were taken in intervals of 15 min during the first hour, and 30 min for the next 3 h. The polymer was precipitated with diethyl ether and the Schlenk was washed to remove residues. Then, the polymer was dissolved in methanol and evaporated until dryness. Finally, it was put under vacuum and a foam was formed.

Route 2

500 mg of DPA (1 eq.), 220 µL of TFA and 0.5 mL of absolute EtOH were stirred in a vial for 10min. After, 1.7 mg of AIBN and 14.4 mg of CPADB were added separately with EtOH (1:5 AIBN/RAFT). The AIBN solution was first transferred to the vial with CTA, and the resulting mixture transferred to the vial containing the monomer. In each transfer the vials were washed with EtOH. Finally, the mixture was transferred to a Schlenk tube and left under argon

atmosphere. The total volume of EtOH was 1.8 mL. The oxygen was removed with five freeze-pump cycles. The mixture was then placed in an oil bath at 80 ℃ for 5h. The polymer was precipitated with diethyl ether and the Schlenk was washed to remove residues. Then, the polymer was dissolved in ethanol and evaporated until dryness. Finally, it was dried under vacuum and a solid product was formed.

2.2.6. Polymer grafting to the MSN surface

A Schlenk tube (A) was prepared containing 100 mg of MSN4+CPADB and 0.27 mg of AIBN (molar rario AIBN/RAFT: 1:5) under argon atmosphere. In a separate Schlenk tube (B) a polymerization reaction was conducted as described for the kinetic study, using two times the quantity of CTA present in the Schlenk A. At 3h (≈55% conversion, see section 3.5.), the mixture from B was transferred to Schlenk A with a cannula under argon and left at 80 ℃ for 24h. (Scheme 5) The particles were recovered by centrifugation at 12000 rpm for 10 min at 18 ℃., and washed three times with absolute ethanol, keeping each supernatant. The solid product obtained was dried at 50 ℃ overnight. Finally, the particles were dried under vacuum. The polymer present in the supernatant was precipitated with diethyl ether. After, the polymer was dissolved in ethanol and dry under vacuum and a solid product was formed.

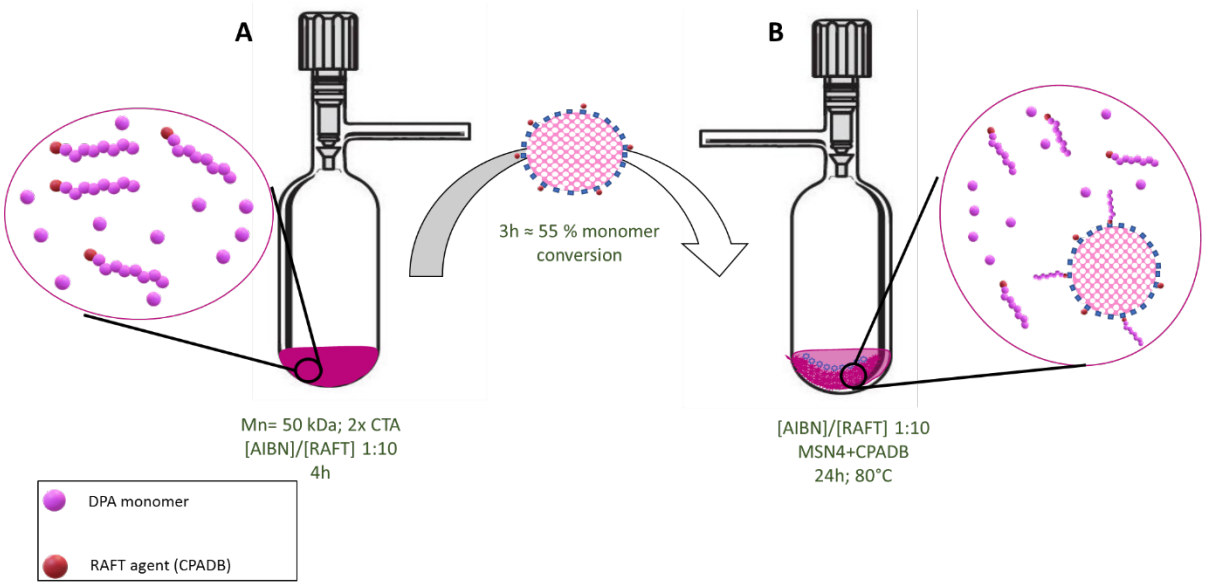

Scheme 5 - Schematic ilustration of the procedure to graft polymer to MSN surface.

2.2.7. Loading and release of Sulphorhodamine B

For loading and release of SRB, a ethanolic solution of SRB (3.90×10^{-3} M, 500 µL) was added to 1.5 mg of MSN+PolyDPA, and the dispersion was stirred overnight at room temperature. The dispersion was centrifuged (15000 rpm, 10 min at 20 ℃) to remove the unloaded SRB. The SRB loaded nanoparticles were redispersed in 1 mL of phosphate buffer (pH 9) and centrifuged. This procedure was repeated one more time, recovering the supernatants. After the last centrifugation, he supernatant was removed and 200 µL of PBS (pH 9) was added to the loaded nanoparticles. The mixture was transferred to the dialysis device (compartment A, scheme 6) and inserted on

top of the fluorescence cuvette (previously filled with 3.2 mL of PBS (pH 9)), immediately before the beginning of the experiment. (Ribeiro et al. 2017) (scheme 5) SRB released from the nanoparticles was monitored through the fluorescence intensity of SRB ($\lambda_{excitation} = 566\ nm; \lambda_{emission} = 589\ nm$) on the bottom compartment of the fluorescence cuvette (compartment B, scheme 6), while modulating the pH between 5 and 9, with additions of H_2SO_4 (1 M, 10 µL) (300 s, 3800 s, 6000 s, 9020 s, 10600 s and 16500 s) and NaOH (1 M, 1 µL) (7880 s and 17700 s) for nearly 6 h. The additions were bottom in compartment A.

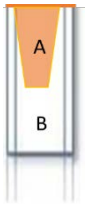

Scheme 6 - Schematic image of the dialysis device used in the release study. The dialysis tube with a cellulose membrane (A) contains 200 µL of PBS pH 9 and 1.5 mg of MSN+PolyDPA with SRB and the fluorescence cell (B) contains PBS pH 9.

3. Results

A novel pH-responsive Control-Release DDS, composed of a silica nanostructure core coated with a pH-responsive polymeric shell, was synthesized. The particles were submitted to amine surface modification process using APTES. These molecules allow to immobilize CTA molecules for the controlled polymerization of DPA from the surface. The polymer shell-coated MSN were obtained using a hybrid grafting approach (Scheme 7).

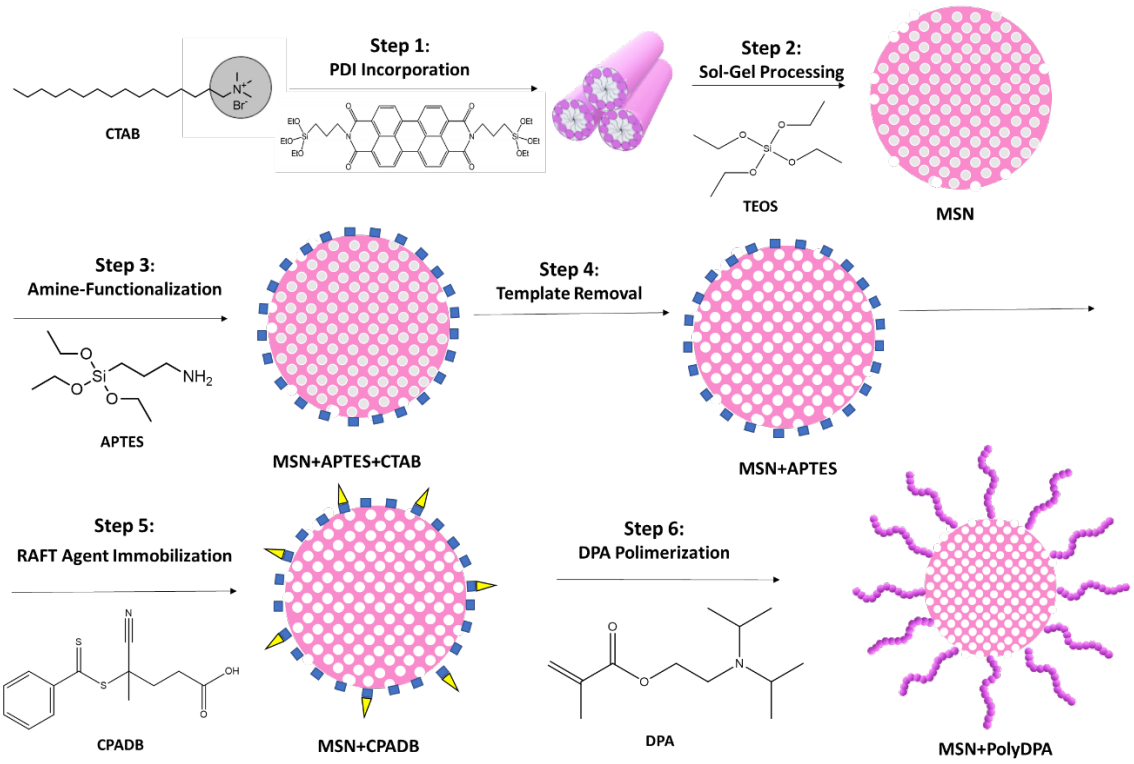

Scheme 7 - Schematic illustration for hybrid mesoporous silica nanoparticles prepared during this work.

3.1. MSNs Synthesis and Characterization

To infer the impact of the pH in MSNs' size, solutions of different [NaOH] were used while maintaining the remain conditions (temperature, stirring, reactants and molar ratios) As mentioned (see section 1.1.3.) higher pH values will produce larger nanoparticles because there will be more OH^- groups (after TEOS hydrolysis) to interact with the positive charges at the micelles surface, decreasing their stability. This charge screening induces the micelle aggregation, increasing the supramolecular aggregation number, and producing larger nanoparticles.

MSNs size distribution was analyzed by TEM, SEM and DLS (20 ℃) in order to estimate their diameters. In Figures 13 to 15 is represented one TEM image of each sample, and the respective diameter distribution. In Figure 16 is showed a SEM image for MSN4 sample, and the respective diameter distribution.

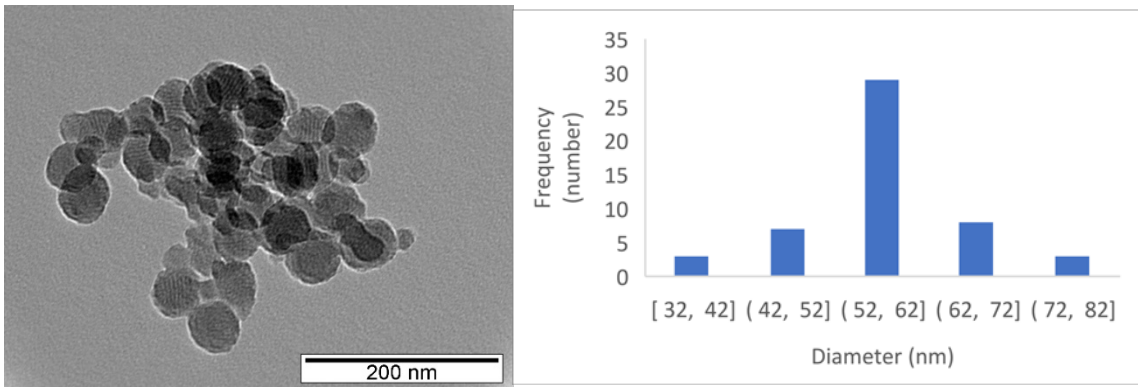

Figure 13 - TEM image (200 nm scale) obtained for MSN1 (left) and its histogram size distribution (right).

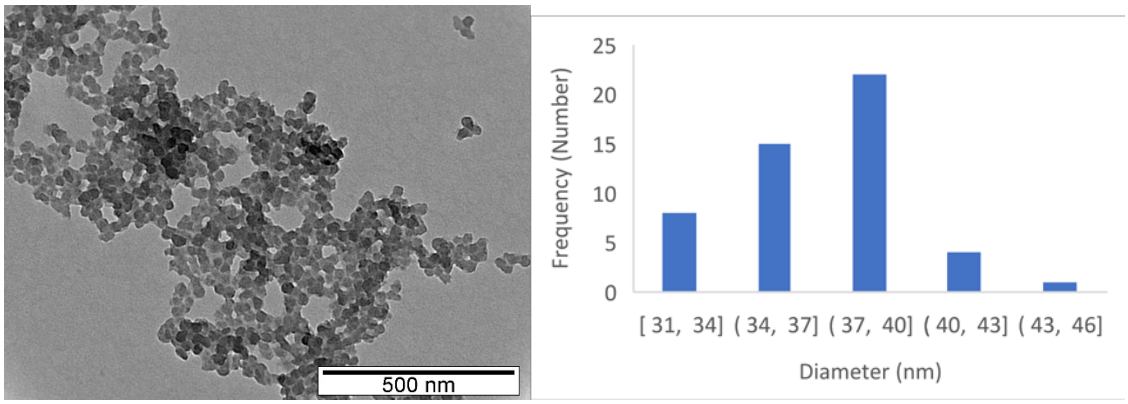

Figure 14 - TEM image (500 nm scale) obtained for MSN2 (left) and its histogram size distribution (right).

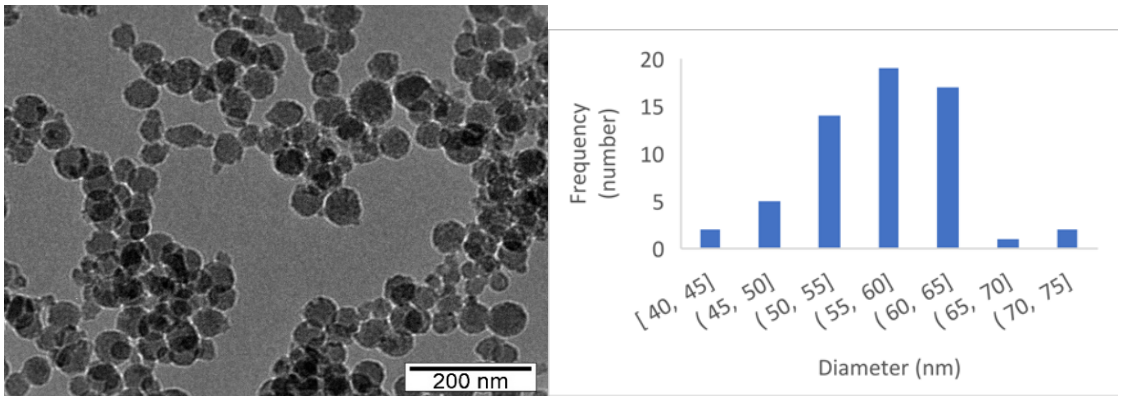

Figure 15 - TEM image (200 nm scale) obtained for MSN3 (left) and its histogram size distribution (right).

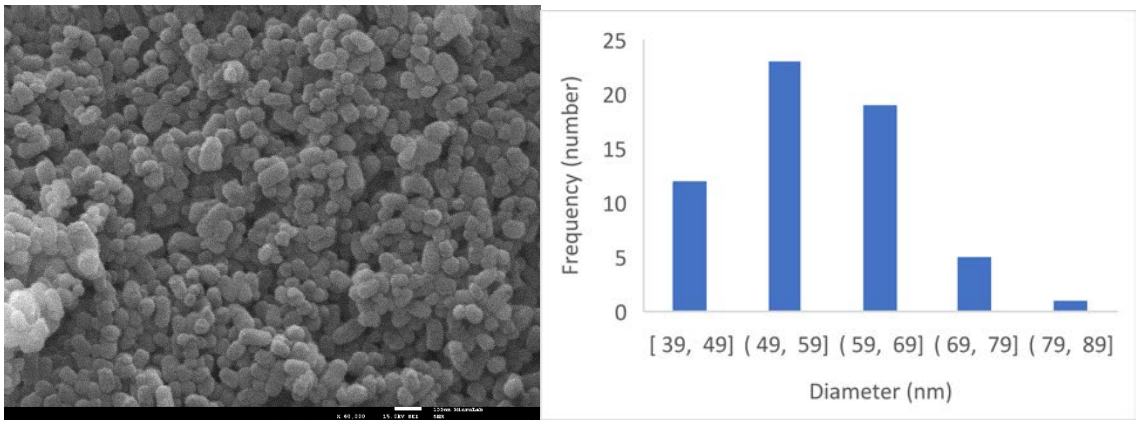

Figure 16 - SEM image (100 nm scale) obtained for MSN4 (left) and its histogram size distribution (right).

The dimensions obtained by the two methods, for each batch, are presented in Table 1.

Table 1 - Particles' size obtain by TEM and DLS and respective standard deviation.

Sample	[NaOH] (M)	D_{TEM} (nm)	D_H (nm)
MSN1	1.7	56 ± 8	198 ± 72
MSN2	1.0	37 ± 3	75 ± 40
MSN3	1.7	57 ± 6	191 ± 21
MSN4	1.7	57 ± 9	182 ± 70

The diameters obtained from DLS are higher than the ones obtained from TEM as expected, since a hydrated layer is formed around MSN when the particles are dispersed. Even though, the values obtained from the two methods are different, both indicate that particles synthesized in the same conditions have identical sizes. MSNs synthesized in higher pH conditions are, as expected, larger than those produced in lower pH conditions. (Chiang et al. 2011)

3.2. Hybrid Nanoparticles

3.2.1. Amine surface modification of the MSNs

After MSN synthesis, an amino surface modification was performed by adding (3-aminopropyl) triethoxysilane (APTES) to the silanol groups of the nanoparticles' external surface (see scheme 6, step 3). In order to assess and quantify the amino incorporation, ^{1}H NMR was performed. This method allows a better quantification of the molecules linked to the particles, due to the action of the base that dissolves the silica matrix. In addition, this method provides a ^{1}H NMR spectra with a higher definition, because of an improvement of the molecules' mobility in solution. (Crucho, Baleizão, and Farinha 2017)

The peak from the alpha-carbon to the silicon atom (less affected by possible interactions of the functional group) was used to estimate the number of organic molecules grafted onto the surface of MSNs, by comparing their integrated intensities with that of the internal standard. (Crucho, Baleizão, and Farinha 2017) In Figure 17 we present the ^{1}H NMR spectra for MSN1+APTES.

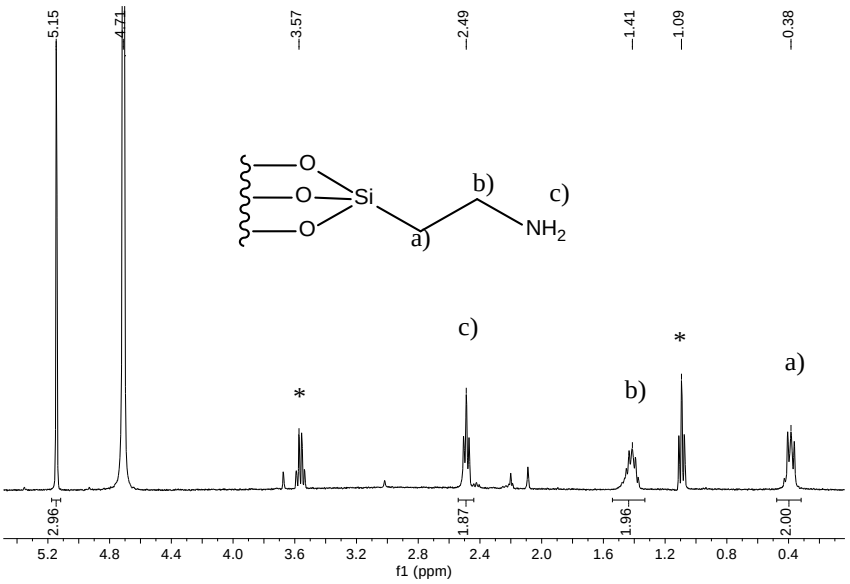

Figure 17 - ^{1}H NMR spectra recorded at 400 MHz of MSN1+APTES in NaOH/D_2O. Ethanol peaks are marked with (*). The internal standard peak is at 5.15 ppm.

The integrated intensity of peak a) was normalized to account the two protons bond to the alpha-carbon. The value for the integrated intensity of the internal standard peak (I_{IS}) was divided by the number of protons of 1,3,5-trioxane. The molar amount of APTES was then calculated since the molar amount of the IS is known:

$$n_{APTES} = \frac{n_{IS}}{I_{IS}}$$

The surface coverage (molecules/nm^2) was calculated from the surface area and volume of a particle and, using a density of 0.34 g/mL for MSN. First, from the mean particle size we calculated the area and volume of the particles. The mass of a particle was calculated from the density and the calculated volume, allowing the quantification of the particles per gram of material. With the number of particles per gram, and the total area of an individual particle, we determine the total area (m^2) per gram. The concentration of the functionalized compound (mol/m^2) can then be obtained from the total area and the value obtained by NMR. From this we obtain the corresponding number of molecules/nm^2. (Crucho, Baleizão, and Farinha 2017)

In Table 2 we present the concentration of APTES on the surface of each particle.

Table 2 - APTES concentration on the MSN surface, calculated by ^{1}H NMR.

Sample	[APTES] (mmol/g MSN)	[APTES] (APTES molecule/nm^2)
MSN1+APTES	2.22	4.25
MSN2+APTES	1.66	2.07
MSN3+APTES	1.50	2.90
MSN4+APTES	2.12	4.10

This amino modification allows the immobilization of other molecules to the external surface of silica, which in this work is a RAFT agent. After this reaction the surfactant was removed by treating the particles with an ethanolic solution of chloridric acid.

3.2.2. Chain Transfer Agent modified MSNs

The RAFT used was BSPA. Its immobilization was achieved by reacting the carboxylic acid with the amine on the surface of the MSN (see scheme 6, step 5). In order to quantify the amount of CTA molecules immobilized on the surface, UV-Vis spectroscopy was used. The RAFT agent exhibit an absorbance maximum around 310 nm. UV-vis spectra of MSN+APTES (previous step) and MSN with CTA attached (MSN+CTA), were measured. (Santiago et al. 2015)

The MSN+APTES spectrum was used as a baseline to account for light scattering. This was possible by using the SOLVER® tool to fit the spectra in the upper (wavelengths higher than 350 nm) and lower (wavelengths lower than 300 nm) regions (Figure 18).

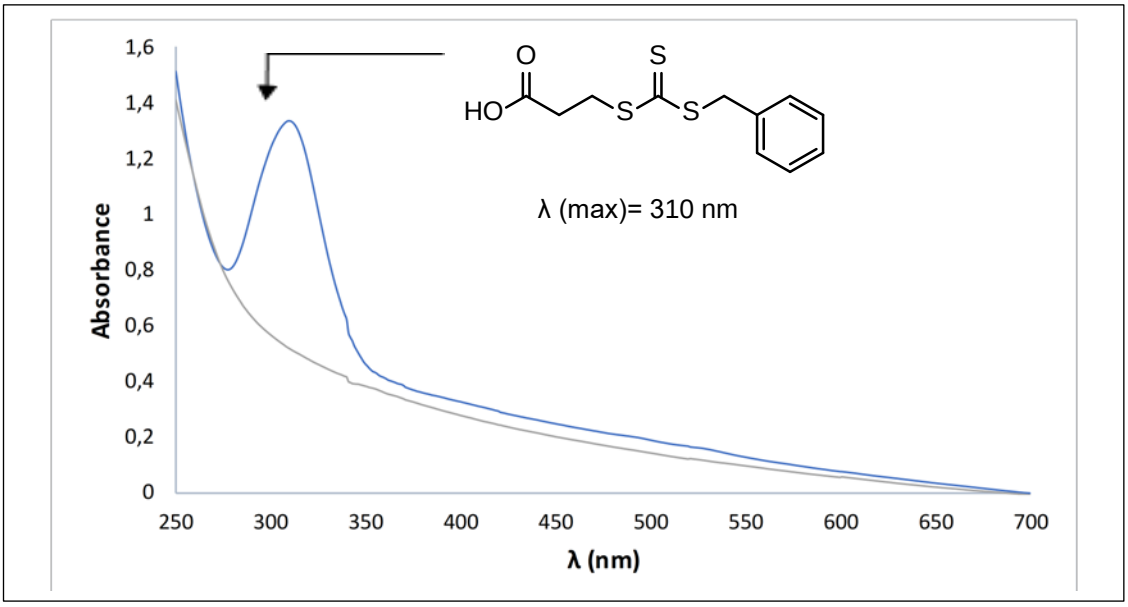

Figure 18 - UV-Vis Spectrum for MSN+APTES adjusted (grey) and for MSN+BSPA (blue).

The first results obtained showed that [CTA] = 5.99×10^{-3} mmol/g MSN (0.11 CTA molecule/nm^2).

These results were surprising because the CTA and the surface ligand were present in equimolar quantities and so, it was expected an agent's concentration close to the one of APTES. This meaning that almost every CTA would react with the ligands present in the particle's surface.

The low CTA concentration was attributed to two factors: the treatment used to remove the surfactant prior to the immobilization of the CTA and stereochemical effects. The treatment to remove the surfactant prompted the protonation of the amine groups reducing their nucleophilic character. Additionality, the attachment of each CTA molecule to the surface may hinder subsequent reactions in its vicinity due to stereochemical hindrance.

Since reducing the impact of the stereochemical effects is not possible without changing the system, in order to increase the quantity of CTA fixated on the surface, the focus was on reverting the loss of nucleophilic character of the amine groups. This way, the particles were washed with an ethanolic solution of ammonia. After this procedure, the initial reaction was performed with MSN1+BSPA.

The CTA concentration in the surface increase when compared to the first reaction, nonetheless, the concentration was significantly lower than the APTES concentration. However, the decision of not pursuing a higher CTA concentration was made because it was reported from Tsujii *et al.* that in RAFT-mediated graft polymerization, termination reactions (recombination) occur with a surprisingly high rate at an early stage for surface densities as lows as 0.08 chains of polymer/nm^2 (i.e. 0.08 CTA molecules/nm^2). This is due to the migration of radical on the surface by sequential chain transfer reactions. By this "reaction-diffusion" mechanism, two active radicals originally far apart from each other can come closer after many steps of the exchange reactions. (Tsujii et al. 2001)

After the preliminary results of the polymerization study (see section 3.4) it was decided to change the RAFT agent. Therefore, a new batch of nanoparticles was functionalized and the new CTA (CPADB) was immobilize by the same process as BSPA.

In Table 3 are presented the concentration of CTA in each particle batch. The difference of concentration of MSN3+CTA is from not being washed with the ammonia solution prior to the addition of CTA.

Table 3 - Concentration of CTA on the surface of the particles.

Sample	[CTA] (mmol/g MSN)	[CTA] (CTA molecule/nm^2)
MSN1+BSPA	1.35×10^{-1}	0.26
MSN2+BSPA	1.66×10^{-1}	0.21
MSN3+BSPA	3.34×10^{-2}	0.06
MSN4+CPADB	8.34×10^{-2}	0.16

3.3. ζ-Potential

In an ionic solution, nanoparticles with a net charge will have a layer of ions strongly bound to their surface; this is referred to as the Stern Layer. A second diffuse outer layer is comprised of loosely associated ions. These two layers are collectively called the electrical double layer. Due

to Brownian diffusion, a potential difference is created between the dispersion medium and the stationary layer of fluid attached to the dispersed particle. The electrostatic potential at this "slipping plane" boundary is called the zeta potential. (Walker 2012)

It is usually used as a key indicator of stability of colloidal dispersions. The extent of the potential indicates the degree of electrostatic repulsion between adjacent, similarly charged particles, therefore, a high zeta potential will increase colloidal stability. Furthermore, it is widely used for qualitative assessment of the charge, which allowed its use as an additional parameter to assess the surface modification at each stage of this work. (Bhattacharjee 2016)

The results are presented in Table 4.

Table 4 - ζ-potential of MSN samples on every step of its surface modification measure.

Sample	ζ-Potential (mV)		
	MSN	MSN+APTES	MSN+CTA
MSN1	-28.0 ± 5.2	29.7 ± 5.2	8.1 ± 3.1
MSN2	-21.0 ± 3.3	30.0 ± 4.0	10.3 ± 3.1
MSN3	-13.0 ± 4.5	30.0 ± 4.8	30.2 ± 4.9
MSN4	-20.2 ± 3.3	28.0 ± 4.2	13.4 ± 3.8

It is possible to observe a significant change in each modification step, which is in accordance with the results of the other methods. The bare MSNs without surfactant show a negative potential because the silanol groups have an (IEP) of 1.5, thus having a negative charge at pH higher than 1.5. The APTES-functionalized MSNs show positive potentials due to the presence of the amine function which shifts the Isoelectric Point to higher pH values, as the intrinsic pKa of the aminopropyl is 9.8 and the IEP is 10.6, and the amino groups should be fully protonated at pHs less than about 9. The immobilization of CTA in the MSN surface resulted in a substantial decrease of ζ-Potential, which indicates a successful surface modification. However, in the case of MSN3+CTA there was no ζ-Potential alteration. This can be explained by the low amount of CTA grafted onto the surface. (Rosenholm and Lindén 2008; Santiago et al. 2015)

3.4. Polymerization Study

Prior to coating the MSNs with a polymer shell, it was necessary to confirm that the chosen RAFT agent (BSPA) was, indeed, controlling the polymerization, e.g., the targeted average number molecular weight (M_n) was achieved. Furthermore, the reaction's kinetic should be determined to ascertain the optimal reaction conditions.

For this purpose, the polymerization was conducted in solution in the conditions presented in Table 5. These conditions were chosen because they were reported to be used in RAFT polymerization of a DPA-containing copolymer. (Hu et al. 2007)

A scheme of the RAFT process with this class of agent is presented in Scheme 8. The mechanism is similar to the one explained before (see section 1.2.2., Scheme 1) but applied to the

trithiocarbonate type RAFT agent used in these polymerizations. The R group is a benzyl and the Z group is a carboxylic acid.

Table 5 - Conditions used for polymerization in solution of monomer DPA.

Experiment	1	2
Temperature (℃)	80	90
Solvent	Dioxane	
$V_{solvent}$ (mL)	1	
Initiator	AIBN	
[Initiator]/[CTA] ratio	1/10	
$[CTA]_0$ (M)	0.7	
$[DPA]_0$ (M)	0.7	
Expected M_n (kDa)	10	

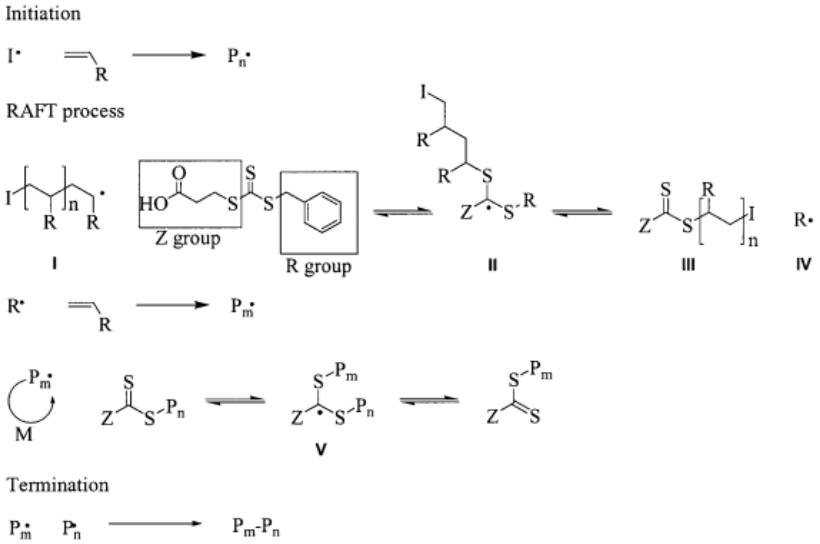

Scheme 8 - Mechanism of the RAFT process with trithiocarbonates. (Stenzel and Davis 2002)

The kinetics of the reaction was followed by ^{1}H NMR as shown in Figure 19.

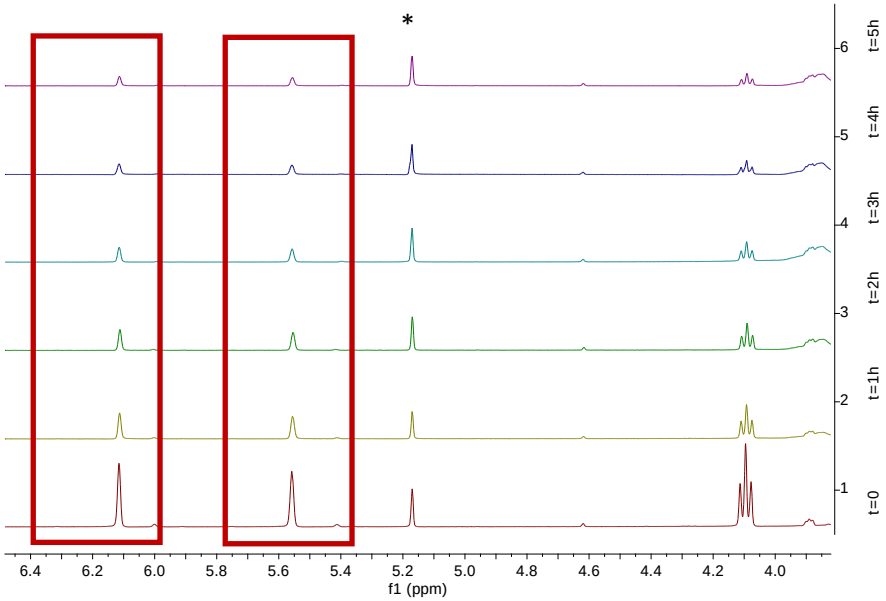

Figure 19 - ^{1}H NMR of the reaction samples in solvent $CDCl_3$. The internal standard peak is marked with (*).

It is evident the disappearance of the peaks at 5.56 ppm and 6.10 ppm corresponding to the vinylic protons along the time reaction. It is also noteworthy the shifting of the peak corresponding to the "aliphatic" protons of the Esther from 4.07 to 3.87 ppm along the time reaction.

The reaction's conversion was determined using 1,3,5-trioxane as the internal standard, and are presented in Figure 20.

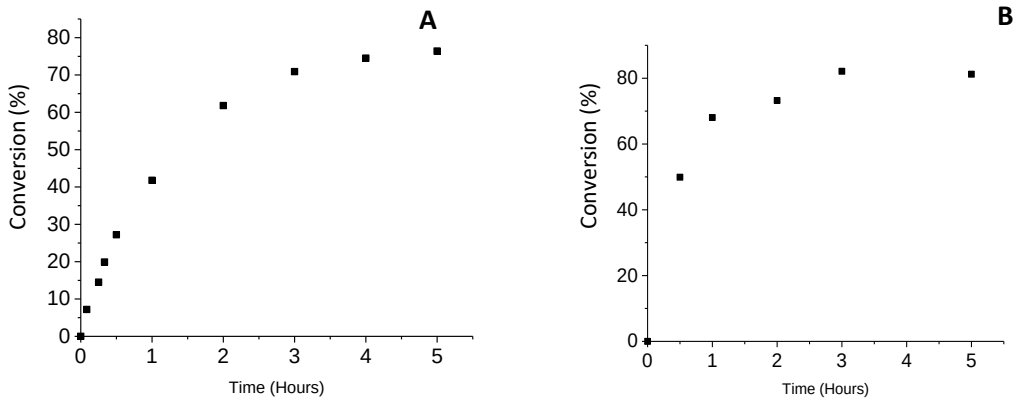

Figure 20 – Polymerization kinetics at T = 80 ℃ (A) and at T = 90 ℃ (B).

From these results it was possible to conclude that the reaction is faster at a higher temperature, but the final conversion is similar. Moreover, after 4h the conversion does not increase significantly. Consequently, it was decided to do the polymerization at 80 ℃ during 4h.

The number average molecular weight of the polymer was initially determined by Gel Permeation Chromatography Multi Angle Light Scattering (GPC-MALS).

The data obtained from GPC-MALS is presented in Figure 21. The shape of curve A gives an indication of the quality of the sample. A more irregular curve will give inaccurate results but can give information about the presence of aggregates. Curve B gives the molecular weight as a function of the elution. For a perfect monodisperse sample, this curve is a straight line.

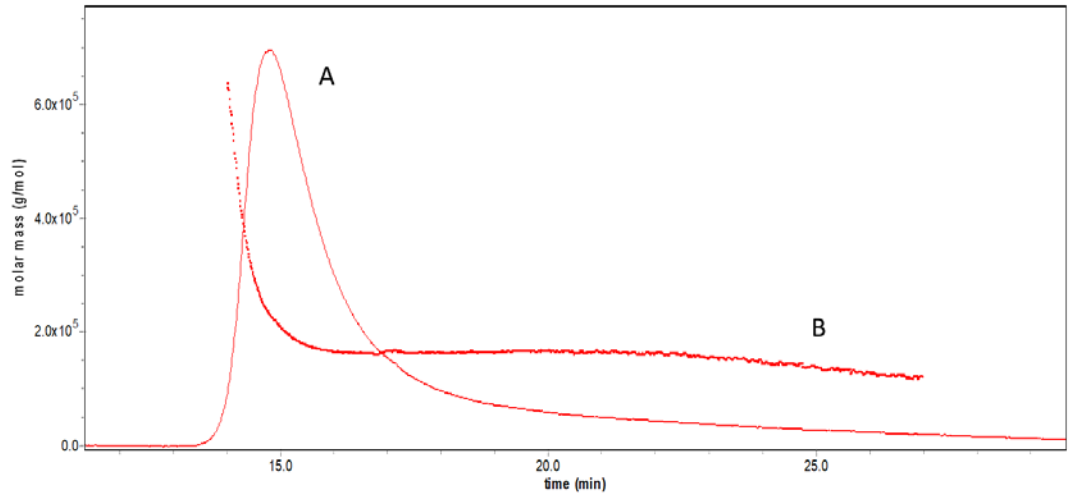

Figure 21 - Chromatogram obtained from GPC-MALS of a PolyDPA sample. (A) Raw data from the detector; (B) Molecular weight vs elution time.

Information of the sample's fluorescence can also be obtained from the data from GPC-MALS. This can important, for example, if we want to infer the presence of chromophores. In the present case, the presence of the RAFT agent is detected (Figure 22, green curve)

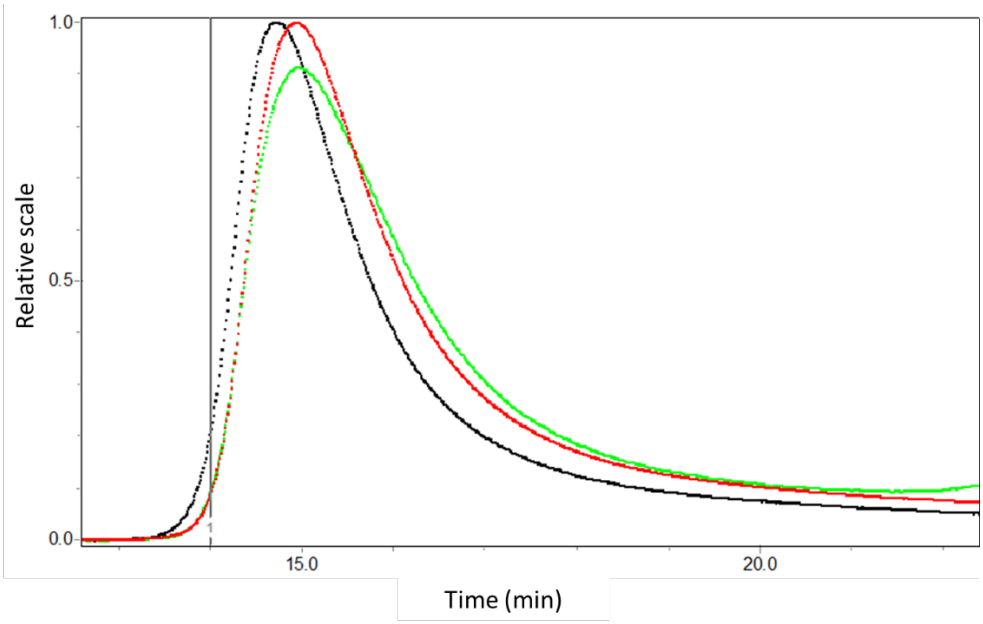

Figure 22 - Data obtained from GPC-MALS for a PolyDPA sample: raw data from the detector (black curve); fluorescence of the sample (green curve); refractive index data (red curve).

In addition to GPC-MALS, UV-Vis spectroscopy was used to determine M_n. By measuring the absorbance of a sample of PolyDPA the concentration of RAFT agent is determined. Knowing the exact concentration of the sample and considering that each polymeric chain has only one CTA molecule is possible to calculate M_n. (Figure 23) This method is a faster method to determine the molecular weight of our polymer, and it can be used without GPC because it provides a similar value for M_n. The major drawback is that it does not provide the size dispersity ($Đ$).

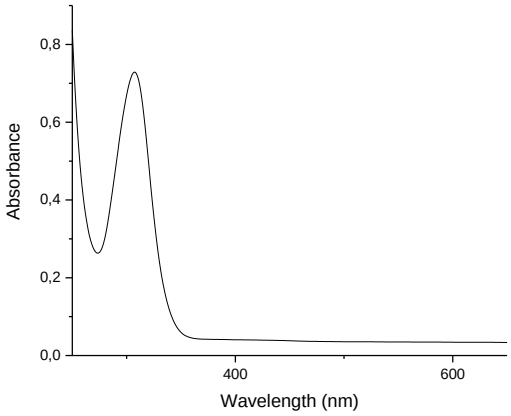

Figure 23 – UV-Vis spectra of a sample of PolyDPA.

The molecular weights for experiments 1 and 2 are shown in Table 6, along with $Đ$ which is the ratio of weight average molecular weight (M_w) and number average (M_n).

Table 6 – Mn and Polydispersity Index results obtained by GPC and the Mn obtained by UV-Vis.

Experiment	1	2
M_n^{GPC} (kDa)	185	142
M_w^{GPC} (kDa)	198	154
$Đ$	1.07	1.09
M_n^{UV-Vis} (kDa)	217	164

On one hand, the polymerization is being controlled because size dispersity is very close to 1. On the other hand, the obtained M_n is very high. The conjugation of these two factors lead to the conclusion that only a fraction of the CTA (~7%) was taking part in the reaction and that the remaining was being deactivated.

A possible explanation was that the RAFT agent was degraded. ^{1}H NMR of the RAFT (1h at 80 ℃) was performed confirmed that the agent was not degraded, which discarded the hypothesis.

The next possibility was that, considering the structures of the BSPA and of the DPA monomer, it was possible that the later was interacting with the former and, consequently, deactivating it. A similar situation was reported describing an amino-containing monomer that degraded the trithiocarbonate chain-end group at high temperatures. (Abel and McCormick 2016) The ^{1}H NMR of BSPA+DPA (1h at 80 ℃) did not show any alteration in the CTA's structure. This means that, possibly, the deactivation only occurs once the polymerization is initiated. In order to prevent a possible interaction, it was decided to protonate the amine of the monomer. For this purpose, we used 1.25 CTA eq. of Trifluoroacetic Acid (TFA) in the subsequent polymerizations. (Table 7)

Table 7 - Conditions used for polymerization in solution of monomer DPA.

Experiment	3	4	5	6
Temperature (℃)	80			
Solvent	Dioxane	Ethanol		
$V_{solvent}$ (mL)	3	1		
[AIBN]/[CTA] ratio	1/10			
$[CTA]_0$ (M)	0.7	2.1		
$[DPA]_0$ (M)	0.7	2.1		
Expected M_n (kDa)	10			2.5

The addition of TFA led to the formation of positively-charged polymeric chains. This changed the interaction of the polymer with the columns of GPC and was not possible to run a GPC with these samples. Therefore, the polymer's number average molecular weight was determined solely using UV-Vis spectroscopy. The results are displayed in table 8.

Table 8 - Mn obtained by UV-Vis.

Experiment	3	4	5	6
M_n^{UV-Vis} (kDa)	82	77	79	46

From the results can be concluded that this RAFT agent is not suitable for the polymerization of this monomer. In experiment 6 the target M_n was lowered to see if there was some proportionality between the target and the obtained M_n.

Since the most suitable pH-responsive polymers have amino groups, it was decided to change the RAFT agent. A dithiobenzoate (CPADB) was chosen because it was reported to work with a DPA-containing copolymer. In addition, this type of CTA exhibits a sufficient addition reactivity even towards less reactive radicals like methacrylate. (Favier and Charreyre 2006; Hu et al. 2007)

New experiments were made to determine the optimal conditions for the reaction with the new RAFT agent. The conditions are presented in table 9.

Table 9 - Conditions used for polymerization in solution of monomer DPA.

Experiment	7	8
Temperature (℃)	80	
Solvent	Ethanol	
$V_{solvent}$ (mL)	1.8	
Initiator	AIBN	
[AIBN]/[CTA] ratio	1/10	1/5
$[CTA]_0$ (M)	1.3	
$[DPA]$ (M)	1.3	
Expected M_n (kDa)	10	

In experiment 7 no polymer was obtained which can be attributed to the death of the intermediate radicals since CPADB is more prone to side reactions than BSPA. In experiment 8 there was

formation of polymer with an M_n = 12.8 kDa. This proved that CPADB was a suitable CTA to this monomer.

These experiments were followed by another kinetic study, necessary due to the change of RAFT agent and the addition of TFA. The study was performed as described before (see section 2.2.5.) The results obtained are in line with the literature. (figure 24)

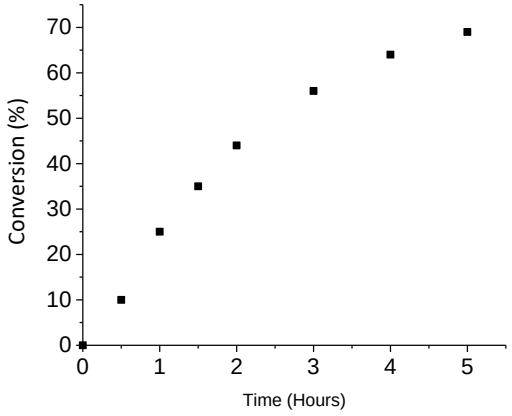

Figure 24 - Polymerization kinetics obtained for the new system.

3.5. Nanoparticles with a pH-responsive shell

The study of the polymerization reaction in solution not only allowed the determination of the optimal reaction conditions but, most importantly, to detect that the initial CTA was not a suitable choice for this monomer. With the data collected, the next step was to create a polymer shell around the MSNs.

The approach idealized to modify the nanoparticle surface with a polymer was the “grafting from” method, in which, only anchored RAFT agents would mediate the polymerization. However, non-published results of our group indicated a low incorporation of polymer using this method. Furthermore, it was reported that the addition of free RAFT agents in solution resulted in a increased polymer incorporation. This CTA excess in the polymerization mixture helps in exchanging oligomeric radicals between the grafted RAFT agents and in solution. In addition, it helps to decrease the cross termination of the polymeric radicals. (Kutcherlapati and Koyilapu 2017)

With all this considered, the initial strategy was abandoned, and it was decided to use this approach, a hybrid grafting method. Aside from providing a higher polymeric grafting it also offers an opportunity to characterize the polymer grafted without destroying the particles, using the polymer that remains in the polymerization medium.

A sample from the mixture of Schlenk A (see section 2.2.6., scheme 5) was taken and ^{1}H NMR was performed to determine the monomer conversion when the polymerization in solution was stopped, which was 50 %.

In Table 10 we present the molecular weight obtained as well as the amount polymer incorporated by mass of particles (determined by 1H NMR) and the equivalent number of chains by particle. In this case it was possible to obtain the molecular weight by GPC by cooling the columns.

Table 10 - Molecular weight of the polymer incorporated in the MSN obtained by GPC and UV-Vis, size dispersity, the amount of polymer incorporated.

	M_n^{Target} (kDa)	M_n^{GPC} (kDa)	$Đ$	M_w^{GPC} (kDa)	M_n^{UV-Vis} (kDa)	Polymer Incorporation (wt% polymer/MSN)
MSN4+PolyDPA	50	55	1.04	57	64.4	5.2

From the results is possible to confirm that the polymerization is being controlled because the $Đ$ is low and the M_n obtained are very close to the target. Is expected that the polymeric chains grafted on the surface are homogeneously dispersed and are enough to ensure a good coverage of the surface and, consequently, a reliable controlled delivery system.

The variation of hydrodynamic diameter (D_H) with pH for MSN4+PolyDPA was measured by DLS. (Table 11) For pH values lower than the pKa of the polymer shell, the polymer is in an expanded random coil conformation, with a D_H = 439 nm (diameter value much larger than those of bare MSN). For pH values above the pKa the polymer shell collapses into a globule-like conformation and the size should be similar the one of bare particles. However, it was not possible to measure this diameter, since with a collapsed shell the particles tend to aggregate. (see appendix). The ζ-Potential was also measured in the same conditions of the previous measurements. The result gives further proof for the presence of a polymeric shell, since there is a significant change of the ζ-Potential when compared to the one of MSN4+CPADB (see section 3.3., table 4) The samples were made in milliQ water which has a pH around 5.5. Since the polymer has a pKa of 6.5, the ζ-Potential is positive because the shell is positively-charged.

Table 11 - Values of the D_H and Zet0a potential of MSN4+PolyDPA at pH values lower than pKa.

	Size (nm)	ζ-Potential (mV)
MSN4+PolyDPA (pH<pKa)	439 ± 52	18.3 ± 1.5

3.6. Release Study

The aim of this proof of concept study was to test the controlled release of SRB (Figure 25) incorporated in MSN4+PolyDPA. SRB was used due to its high quantum yield and water solubility. The control was achieved by modulating the pH.

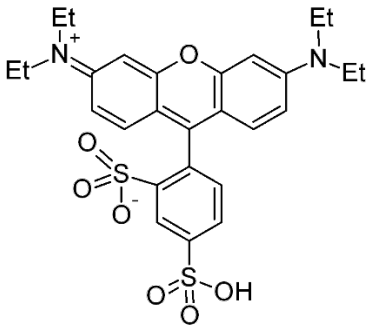

Figure 25 - Structure of SRB.

3.6.1 Incorporation of SRB

One of the main strengths of MSNs in delivery application is the possibility to carry large amounts of payload due to their high intrinsic specific surface areas and pore volumes. Furthermore, the drug loading levels can be rationally controlled, which means that both the drug loading as well as the particle concentration can be used as parameters to control the total drug levels *in vitro* and *in vivo.* There are two main strategies for drug loading, *in situ* during synthesis or as post-sorption (either by physisorption or by chemisorption). The latter is the most common approach to loading drugs into MSNs. This allows independent optimization of structural and physicochemical properties of the carrier and the conditions used for the loading. Incorporation of cargo into silica can be achieved by different means. The one used in this work was physical adsorption from solution into the mesopores, which is the most often used method for the loading of small molecules such as SRB. (M. Rosenholm, Sahlgren, and Linden 2011; Ribeiro et al. 2017)

The silica surface is negatively charged under biologically relevant conditions. Therefore, electrostatic adsorption of positively charged adsorbates is an attractive method for incorporating water-soluble cargo into siliceous MSNs. In the present case, the presence of the positively-charged polymer shell not only ensure that the cargo was not prematurely released but also helped the adsorption of the negatively-charged SRB.

In order to determine the molar absorption coefficient (ε) of SRB, several solutions were prepared in PBS at pH 9 and their absorption spectra were determined. (Figure 26)

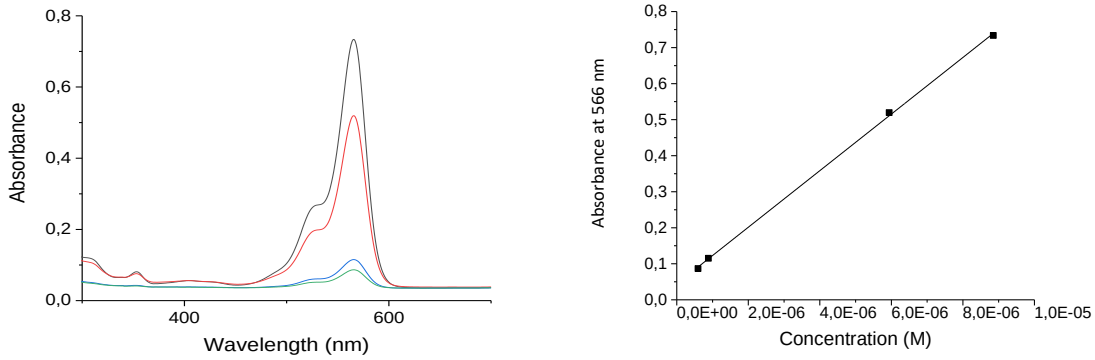

Figure 26 - Absorption Spectra of solutions of SRB in PBS, pH 9: black: C=8.85×10^{-6} M; red: C=5.94×10^{-6} M; blue: C=8.85×10^{-7} M; green: C=5.94×10^{-7} M (left) and respective calibration curve (right).

The calibration curve equation is: $Abs_{máx} = (7.85 \pm 1.2) \times 10^2 \times C + (0{,}044 \pm 0.006)$. From the slope we obtain ε. The Y-interception of the calibration curve is different from zero due to the interferences of the solvent and of the glass from the cuvette, in the optical course.

With this data it was possible to determine the concentration of SRB in the supernatants obtained after the loading process.

The loading process consisted of placing the dry nanoparticles in contact with a concentrated ethanolic solution of SRB. In these conditions, the polymeric shell is positively-charged because the polymerization was done in acidic conditions and the amine is protonated. Therefore, the polymer chains are expanded, allowing the SRB to diffuse into the MSN pores. After loading overnight, the pH was kept at 9 during washing with PBS (pH 9) to remove the SRB molecules adsorbed to the external surface of the nanoparticles. At this pH value the polymer chains collapse, minimizing leakage from the mesopores.

Then, it was possible to determine the amount incorporated into the MSN4+PolyDPA. The number of moles of SRB in each supernatant were determined (Table 12). The amount incorporated was calculated from the difference between the initial quantity used in incorporation and the sum of the quantities present in the supernatants (Table 13).

Table 12 – Number of moles of SRB in the supernatants for each sample.

	$n_{Supernatant\ 1}$ (mol)	$n_{Supernatant\ 2}$ (mol)	$n_{Supernatant\ 3}$ (mol)
MSN4+PolyDPA	9.48×10^{-7}	2.02×10^{-7}	4.53×10^{-8}

Table 13 - Number of moles of SRB used in incorporation, in the supernatants and percentage of incorporation.

	$n_{initial}$ (mol)	$n_{total\ supernatants}$ (mol)	n_{SRB} (mol/g particle)
MSN4+PolyDPA	1.95×10^{-6}	1.19×10^{-6}	7.67×10^{-4}

In the present work the polymeric shell is particularly useful since the incorporation process is done in a medium were the shell is positively charged. This attracts the negatively charged SRB and increases the rate of diffusion. However, the drawback is that a significant amount of SRB molecules are trapped at the polymeric shell and are washed out afterwards.

The release study consisted in changing the polymer shell as a response to a pH alteration. Since the polymer's pKa is about 6.5, we decided to modulate the pH of the dispersion of MSN4+PolyDPA (see section 2.2.7) between 5 and 9. (Kristoffersen et al. 2014)

The emission ($\lambda_{excitation} = 566\,nm$) and excitation spectra ($\lambda_{emission} = 589\,nm$) of SRB in PBS pH 5 and pH 9 (Figure 27) show the dependence of the SRB's quantum yield wtih pH.

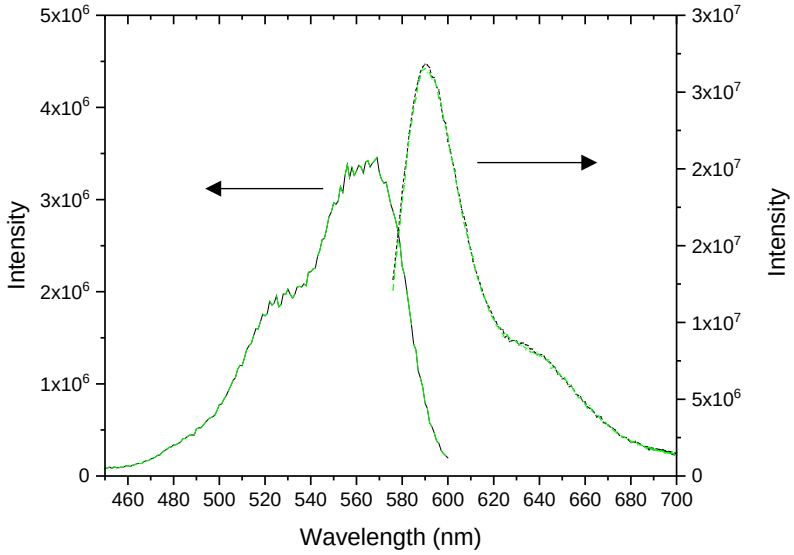

Figure 27 – Emission (dash, right) and excitation (lines, left) spectra of SRB at pH 5 (black) and pH 9 (green), with $\lambda_{\text{excitation}} = 566$ nm and $\lambda_{\text{emission}} = 589$ nm.

As it is possible to observe in Figure 27, It is possible to observe that the SRB's quantum yield is independent from pH within the range used in this study, which is in agreement with the literature. (Coppeta and Rogers 1998)

3.6.2. Controlled Release

To monitor the release of SRB from the nanoparticles we used a fluorescence cuvette fitted with a top chamber separated from the bottom compartment by a dialysis membrane (see section 2.2.7., scheme 5). It was important to determine the influence of pH in the dialysis device, specifically, how it impacted the diffusion across the membrane. A solution of SRB in PBS (pH 9) ($C = 4.37 \times 10^{-6}\,M$) was loaded into the dialysis device and the fluorescence intensity was monitored for 4 h, with additions of 10 µL [H_2SO_4] = 1M every hour. This changes the pH from 9 to 5 in the dialysis device, while the intervals between the additions ensure that the equilibrium is restored and the pH in the device is, again, close to 9. No addition was made during the first hour (Figure 28).

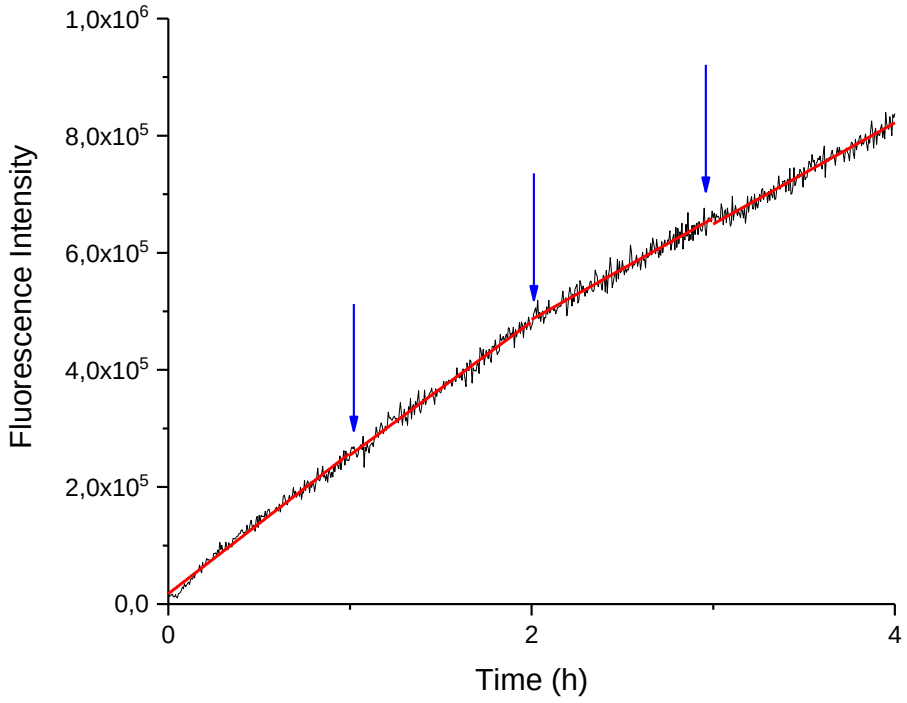

Figure 28 - Evolution of fluorescence intensity in compartment B due to the diffusion of free SRB from compartment A (see section 2.2.7, scheme 6) (black line), indication of acid additions (blue arrows) and linear fit of each section (red lines). $\lambda_{excitation} = 566$ nm and $\lambda_{emission} = 589$ nm.

From Figure 28 it is possible to conclude that pH has no influence in the diffusion process across the cellulose membrane. A linear fit in each section of the kinetic curve, corresponding to each acid addition, provides additional proof of the independence of the diffusion process from pH since the slops have similar values (Table 14). This means that there is no change in the rate of diffusion when the pH changes. The slight declining of slop values along time can be explained by the deacceleration of SRB diffusion, due to the diminishing of the gradient of concentrations between the two compartments.

Table 14 - Values of the slop of the curves for each section of the kinetic curve, and the corresponding error.

Diffusion Time	Slope Value
1 h	$(2.4 \pm 0.2) \times 10^5$
2 h	$(2.3 \pm 0.3) \times 10^5$
3 h	$(1.7 \pm 0.3) \times 10^5$
4 h	$(1.7 \pm 0.3) \times 10^5$

To evaluate the degree of control over cargo release for the MSN4+PolyDPA we used the process described in chapter 2 (section 2.2.7).

The degree of control over cargo release obtained for the nanoparticles was evaluated by continuously measuring the fluorescence of the cuvette, while modulating the pH between 5 and 9 in the dialysis device. The initial strategy was to make acid additions in the dialysis device, to low the pH from 9 to 5. These additions were to be sufficiently spaced to give time to the equilibrium to be restored, and the pH in the dialysis device return to a value close to 9 (Scheme 9).

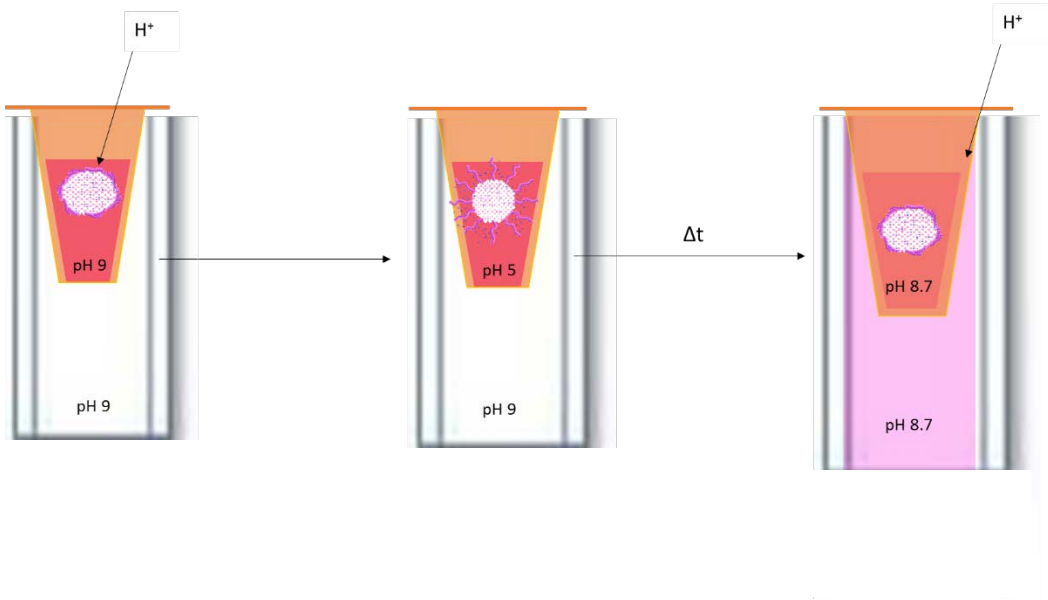

Scheme 9 - Schematic ilustration of the effect of acid addition in the dialysis device.

It was expected to observe an increase in the fluorescence intensity at pH 5 (expanded polymeric chains, pores are open) and a stagnation once the equilibrium was restored and the pH value was closed to 9 (collapsed polymeric chains, closed pores).

The curve obtained through the monitorization of the fluorescence intensity in compartment B is presented in Figure 29, with indication of the acid (black arrows) and base (green arrows) additions. In red is presented a linear projection of the stagnation periods. A zoom of sections A, B, C and D is displayed in Figure 30.

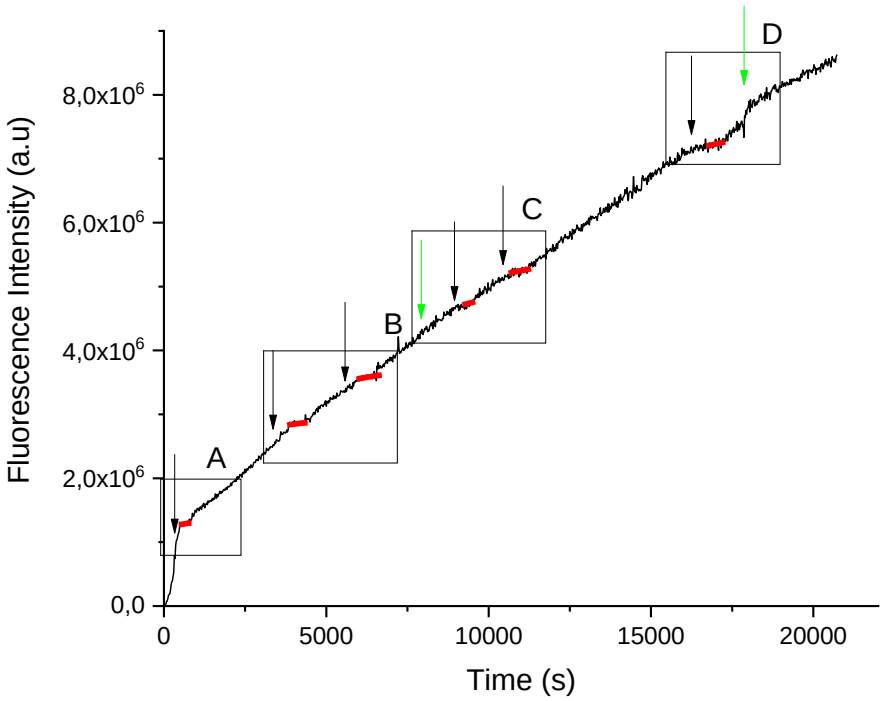

Figure 29 - Evolution of fluorescence intensity in compartment B and indications of acid additions (black arrows) and base additions (green arrows). $\lambda_{excitation} = 566\ nm$ and $\lambda_{emission} = 589\ nm$.

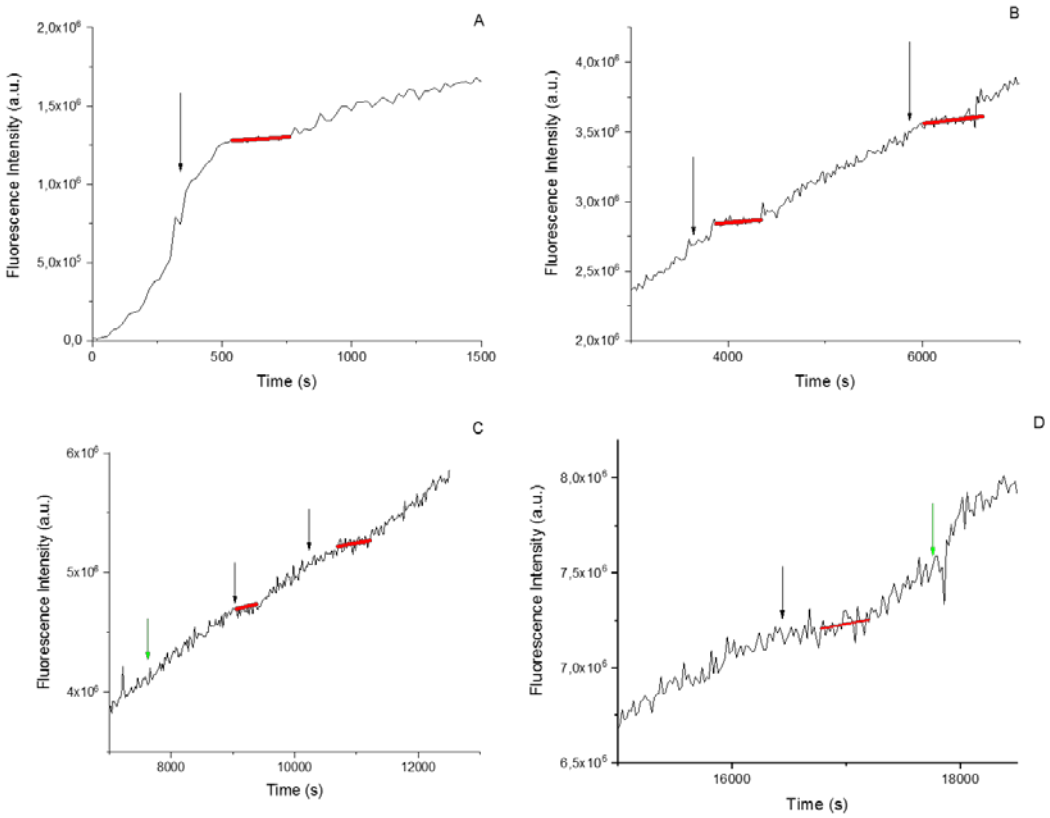

Figure 30 - Zoom of sections A, B, C and D of the evolution of Fluorescence Intensity curve (Figure 29) and indications of acid additions (black arrows) and base additions (green arrows).

From Figure 29 it is possible to observe that the system is working opposite to what was expected, i.e., the fluorescent intensity increases when the pH value surpasses the pKa of the polymer (pH>6.5) and, stagnates when acid was added (pH 5). This can be explained by the characteristics of the polymer shell and of the cargo used. After each acid addition the pH decreases to 5 (pH below the polymer pKa) and the shell is protonated, and it expands allowing negatively-charged SRB molecules to diffuse from the mesopores to the polymer shell. Due to the electrostatic interactions SRB molecules are trapped in the shell and are only released when the pH rises (above pKa) to reach equilibrium and the shell is deprotonated (collapsed). This explains why the fluorescent intensity stagnates after each acid addition. It is possible to observe a more pronounced release (Figure 30A) in the beginning due to the presence of SRB molecules adsorbed at the surface. Finally, it is noteworthy that the additions of base had no impact in the system, since the additions were made in periods where the fluorescence intensity is increasing, e.g., the chains are already deprotonated and the base has no effect.

Most important, the results obtained show that the hybrid system is able to control the release of its cargo by changing its polymer shell conformation as a response to pH changes.

To determine the amount of SRB released throughout the experiment and, more specifically, to determine the rate of release before and after the additions of acid and base, a calibration curve was constructed with the values of fluorescence emission ($\lambda_{excitation} = 566\ nm$) as a function of the concentration (Figure 31).

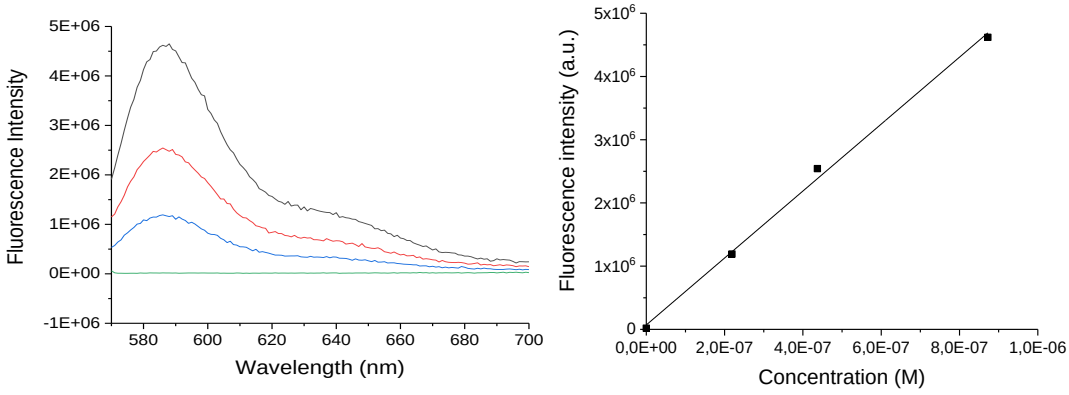

Figure 31 - Emission Spectra ($\lambda_{\text{excitation}} = 566\ \text{nm}$) of solutions of SRB in PBS, pH 9: black: C=8.73×10^{-7} M; red: C=4.37×10^{-7} M; blue: C=2.19×10^{-7} M; green: PBS (pH 9) (left) and respective calibration curve (right).

The calibration curve is: $Intensity_{Fluo} = (5.3 \pm 0.2) \times 10^{12} \times \mathrm{C} + (0.7 \pm 1.0) \times 10^{5}$.

With this curve, and since the volume in compartment B (see section 2.2.7., Scheme 5) is constant, it was possible to obtain the evolution of the number of moles released during the experiment. In the end of the experiment the amount of SRB released corresponded to 2% (mol) of the SRB incorporated, which is an indication that the system is able to control the release process for a long period of time.

The release curve (Figure 29) was divided by sections, corresponding to the periods where the pH was lower (stagnation periods) and higher than the polymer's pKa. Since the volume in the bottom compartment of the dialysis device is constant, it was possible to obtain the rate of release. (Figure 32)

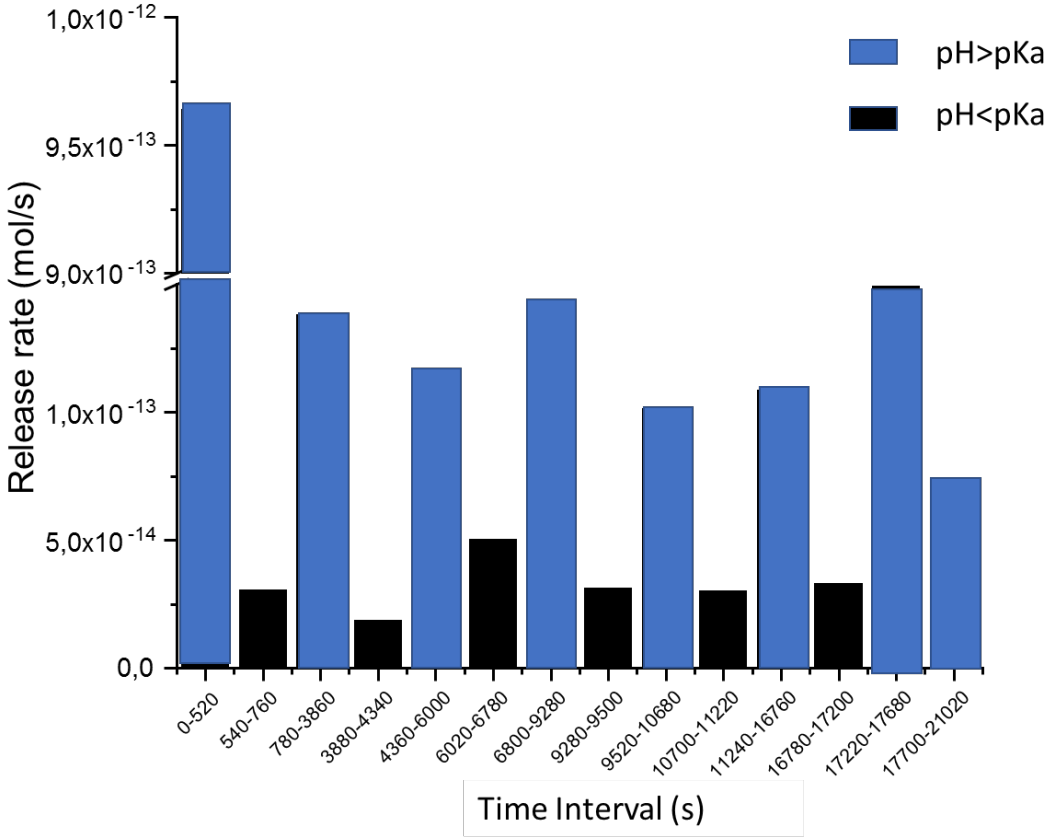

Figure 32 - Rate of SRB release of each section.

The data presented in Figure 32 confirm the conclusions drawn from the release curve. After each acid addition (pH 5 < pKa, black columns) the release rate abruptly drops. This corresponds to the stagnation periods observe in the release curve (figure 26), when the SRB molecules diffuse from the mesopores and are trapped in the polymeric shell. The interval 6020-6780 s has a slightly higher rate, because accounts for a period where two consecutive additions of acid where made. However, when before the second addition was made, some SRB was already being release.

When the pH is returning to the equilibrium value (pH≈9 > pKa, blue columns) the release rate is much higher. The first interval (0-520 s) corresponds to the release of the SRB adsorbed in the external surface was being released. A high accumulation of SRB can explain the higher release rate of interval 6800-9280 s due to the two short-spaced acid additions. Even though some SRB was released between both additions, it was not enough to release all the SRB diffused after the first addition. The SRB molecules adsorbed deeper in the mesospores have to cross a larger path to reach the external surface, therefore, their diffusion is slower which can explain the relative slow release rate in the final section (Scheme 10).

A representative scheme of the behaviour of the system is presented in Scheme 11.

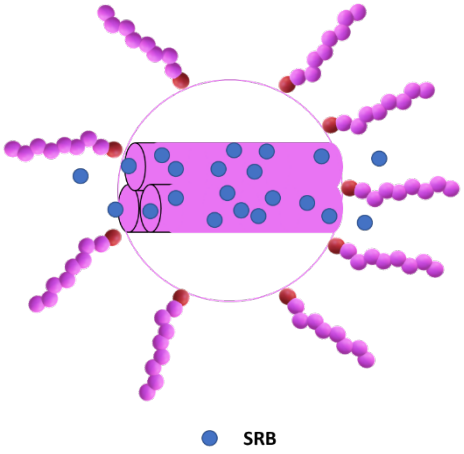

Scheme 10 - Side view of MSN4+PolyDPA during release study.

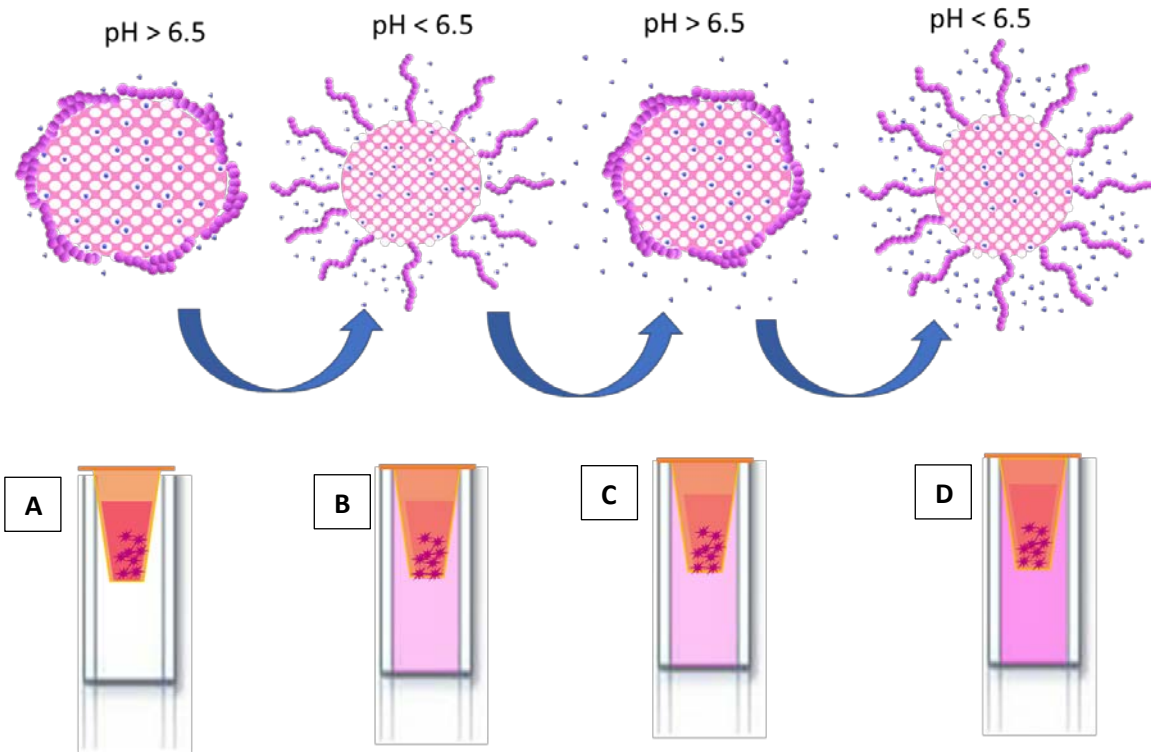

Scheme 11 - Representative scheme of the behaviour of SRB-loaded MSN+PolyDPA. The polymer is expanded at low pH values (B and D) and when the pH rises it collapses (A and C). When the polymer is expanded SRB diffuses to the surface and it is only released when the polymer collapses. Adapted from (Ribeiro et al. 2017).

After each acid addition the pH decreases to 5 (pH below the polymer pKa) the shell is protonated, and it expands allowing negatively-charged SRB molecules to diffuse from the mesopores to the surface. Due to the electrostatic interactions SRB molecules are trapped in the shell. The fluorescent intensity does not increase because there is no SRB diffusion to the bottom compartment (scheme 9, transition B to C).

When the pH increases and surpasses the pKa of the polymer the shell collapses producing a pumping action that releases the cargo. The fluorescent intensity starts to increase again due to SRB molecules diffusion to the bottom compartment (scheme 9, transitions A to B and C to D).

In conclusion, our system is able to control the release of its cargo by changing its polymer shell conformation as a response to pH changes. It presents a low release rate at acidic pH values and a large release rate at basic pH values. This behaviour is not suitable for cancer treatment, since tumour tissues have a more acidic extracellular environment than the corresponding healthy tissues. However, this behaviour can change depending on the cargo's electrostatic nature. It is expected to observe an opposite behaviour for a cargo with no charge, since there will not be interaction with the polymer shell.

The current cancer treatments use highly cytotoxic (neutral) drugs, whose administration is hindered by their low blood stability, decreased bioavailability and lack of specificity, which is responsible for severe side effects. Our system could be a reliable alternative not only to protect the drugs and increase their bioavailability, but also to deliver them in spatial and temporally controlled fashion improving their therapeutic outcome. Moreover, due to the enhanced permeation and retention effect (EPR), this hybrid system can extravasate from the blood stream and accumulate at the tumour tissue. Therefore, we are confident that our system has the potential to be used as a carrier of anti-cancer drugs. (Moreira et al. 2016)

4. Conclusions

In this work a novel carrier for controlled release, based on mesoporous silica nanoparticles coated with a pH-responsive polymer shell, was prepared. TEM and DLS confirmed the success on the synthesis of spherical MSN with narrow size dispersity. Different NaOH concentrations yielded nanoparticles of different sizes due to the electrostatic interaction between OH^- groups (after TEOS hydrolysis) and the positive charges at the micelles surface. The charge screening induces the micelle aggregation, increasing the supramolecular aggregation number, and producing larger nanoparticles.

The particles were submitted to amine surface modification process using APTES. These molecules allow to immobilize CTA molecules for the controlled polymerization of DPA from the surface.

The polymer shell-coated MSN were obtained using a hybrid grafting approach, to increase the polymer incorporation in the particles surface, in comparison with a pure “grafting from” approach. The polymer incorporation was determined to be 5 wt% polymer/particle by ^{1}H NMR. Furthermore, using this hybrid “grafting from” approach it was possible to characterize the incorporated polymer by analysing the chains present in the supernatants. The characterization was made by UV-Vis spectroscopy and GPC-MALS.

In the proof-of-concept release experiments, we use a model molecule (SRB) modulating the pH between 5 and 9. The results show a strong influence of the polymer shell coating on the release kinetics, with the system behaviour being similar to a sponge: the cargo diffuses into the polymer shell at pH values around 5 and is released when the pH rises above pKa (≈6.5) when the shell collapses, producing a pumping action that releases the cargo.

By combining a large cargo capacity and a “smart” pH-actuated release control mechanism, our proof-of-concept hybrid nanocontainers have the potential for application as a nanopumping system in drug delivery,

It should be of great interest to explore how the charge nature of the cargo affects the release kinetics and the cargo incorporation, because a negative-charged cargo (such as SRB) will have a higher affinity with the positively-charged polymeric shell than a neutral or positive one. Furthermore, it is important to study the impact of the polymeric chains length in the polymer incorporation and, consequently, in the release kinetics. Finally, the relation between nanoparticle size and polymer length with its biocompatibility and its effectiveness should be studied.

Once these assays are concluded, it should be interesting to study the drug controlled release *in vitro* to confirm the advantage of using this platform as a future and promising strategy, compared to the conventional treatments currently applied for fighting cancer.

5. References

Abel, Brooks A. and Charles L. McCormick. 2016. “Mechanistic Insights into Temperature-Dependent Trithiocarbonate Chain-End Degradation during the RAFT Polymerization of N-Arylmethacrylamides.” *Macromolecules* 49(2):465–74.

Ahmadi, Ebrahim, Nematollah Dehghannejad, Samaneh Hashemikia, Merajaddin Ghasemnejad, and Hashem Tabebordbar. 2014. “Synthesis and Surface Modification of Mesoporous Silica Nanoparticles and Its Application as Carriers for Sustained Drug Delivery.” *Drug Delivery* 7544(3):164–72.

Amoozgar, Zohreh and Yoon Yeo. 2012. “Recent Advances in Stealth Coating of Nanoparticle Drug Delivery Systems.” *Wiley Interdisciplinary Reviews: Nanomedicine and Nanobiotechnology* 4(2):219–33.

Argyo, Christian, Veronika Weiss, Christoph Bra, and Thomas Bein. 2013. “Multifunctional Mesoporous Silica Nanoparticles as a Universal Platform for Drug Delivery.” *Chemistry of Materials* (26):435–51.

Baeza, Alejandro, Montserrat Colilla, and María Vallet-Regí. 2015. “Advances in Mesoporous Silica Nanoparticles for Targeted Stimuli-Responsive Drug Delivery.” *Expert Opinion on Drug Delivery* 12(2):319–37.

Baleizão, Carlos and J. P. S. Farinha. 2015. “Hybrid Smart Mesoporous Silica Nanoparticles for Theranostics.” *Nanomedicine* 10:2311–14.

Barbhuiya, Salim and Muneeb Qureshi. 2014. *Handbook of Research on Diverse Applications of Nanotechnology in Biomedicine, Chemistry, and Engineering A Volume in the Advances in Chemical and Materials Engineering (ACME) Book Series Book Chapter: Applications of Nanotechnology in Cement and Concrete*.

Barbø, By Christophe, John Bartlett, and Linggen Kong. 2007. “Silica Particles : A Novel Drug-Delivery System.” *Advanced Materials* (21):1959–66.

Beck, J. S., K. D. Schmitt, J. B. Higgins, and J. L. Schlenkert. 1992. “New Family of Mesoporous Molecular Sieves Prepared with Liquid Crystal Templates.” *Journal of the American Chemical Society* (14):10834–43.

Bergström, L. Magnus. 2011. “Thermodynamics of Self-Assembly.” Pp. 289–314 in *Application of Thermodynamics to Biological and Material Science*.

Bharti, Charu and Neha Gulati. 2015. “Mesoporous Silica Nanoparticles in Target Drug Delivery System: A Review.” *International Journal of Pharmaceutical Investigation* 5(3):124.

Bhat, Rajendra R., Michael R. Tomlinson, Tao Wu, and Jan Genzer. 2006. “Surface-Grafted Polymer Gradients: Formation, Characterization, and Applications.” *Advances in Polymer*

Science 198(1):51–124.

Bhattacharjee, Sourav. 2016. “DLS and Zeta Potential - What They Are and What They Are Not?” *Journal of Controlled Release* 235:337–51.

Blanco, Elvin, Haifa Shen, and Mauro Ferrari. 2015. “Principles of Nanoparticle Design for Overcoming Biological Barriers to Drug Delivery.” *Nature Biotechnology* 33(9):941–51.

Cayre, Olivier J. and Simon Biggs. 2011. “Stimulus Responsive Core-Shell Nanoparticles : Synthesis and Applications of Polymer Based Aqueous Systems.” *Soft Matter* (7):2211–34.

Chang, Baisong, Dan Chen, and Yang Wang. 2013. “Bioresponsive Controlled Drug Release Based on Mesoporous Silica Nanoparticles Coated with Reductively Sheddable Polymer Shell.” *Chemistry of Materials* (25):574–85.

Chaudhuri, Rajib Ghosh and Santanu Paria. 2012. “Core / Shell Nanoparticles : Classes , Properties , Synthesis Mechanisms , Characterization , and Applications.” *Chemical Society Reviews* (112):2373–2433.

Chiang, Ya-dong, Hong-yuan Lian, and Sin-yen Leo. 2011. “Controlling Particle Size and Structural Properties of Mesoporous Silica Nanoparticles Using the Taguchi Method.” *The Journal of Physical Chemistry* (115):13158–65.

Chiefari, John et al. 1998. “Living Free-Radical Polymerization by Reversible Addition - Fragmentation Chain Transfer : The RAFT Process.” *Macromolecules* 9297(98):5559–62.

Conde, João, Jorge T. Dias, Valeria Grazú, Maria Moros, and Pedro V Baptista. 2014. “Revisiting 30 Years of Biofunctionalization and Surface Chemistry of Inorganic Nanoparticles for Nanomedicine.” *Frontiers in Chemistry* 2(July):1–27.

Coppeta, J. and C. Rogers. 1998. *Dual Emission Laser Induced Fluorescence for Direct Planar Scalar Behavior Measurements*. Vol. 25.

Crucho, Carina I. C., Carlos Baleizão, and José Paulo S. Farinha. 2017a. “Functional Group Coverage and Conversion Quantification in Nanostructured Silica by 1 H NMR.” *Analytical Chemistry* 89(1):681–87.

Crucho, Carina I. C., Carlos Baleizão, and José Paulo S. Farinha. 2017b. “Functional Group Coverage and Conversion Quantification in Nanostructured Silica by ^{1}H NMR.” *Analytical Chemistry* 89(1):681–87.

Desai, Manisha P., Vinod Labhasetwar, Elke Walter, Robert J. Levy, and Gordon L. Amidon. 1997. “The Mechanism of Uptake of Biodegradable Microparticles in Caco-2 Cells Is Size Dependent.” *Pharmaceutical Research* 14(11):1568–73.

Favier, Arnaud and Marie Thérèse Charreyre. 2006. “Experimental Requirements for an

Efficient Control of Free-Radical Polymerizations via the Reversible Addition-Fragmentation Chain Transfer (RAFT) Process." *Macromolecular Rapid Communications* 27(9):653–92.

Gao, Weiwei, Juliana M. Chan, and Omid C. Farokhzad. 2010. "PH-Responsive Nanoparticles for Drug Delivery." *Molecular Pharmaceutics* 7(6):1913–20.

Grün, Michael, Iris Lauer, and Klaus K. Unger. 1997. "The Synthesis of Micrometer- and Submicrometer-Size Spheres of Ordered Mesoporous Oxide MCM-41." *Advanced Materials* 9(3):254–57.

Hong, Chun-yan, Xin Li, and Cai-yuan Pan. 2007. "Grafting Polymer Nanoshell onto the Exterior Surface of Mesoporous Silica Nanoparticles via Surface Reversible Addition-Fragmentation Chain Transfer Polymerization." *European Polymer Journal* 43:4114–22.

Hong, Chun Yan, Xin Li, and Cai Yuan Pan. 2009. "Fabrication of Smart Nanocontainers with a Mesoporous Core and a PH-Responsive Shell for Controlled Uptake and Release." *Journal of Materials Chemistry* 19(29):5155–60.

Hu, Ying Qian, Min Sang Kim, Bong Sup Kim, and Doo Sung Lee. 2007. "Synthesis and PH-Dependent Micellization of 2-(Diisopropylamino)Ethyl Methacrylate Based Amphiphilic Diblock Copolymers via RAFT Polymerization." *Polymer* 48(12):3437–43.

Ibrahim, Ismail A. M., A. A. F. Zikry, and Mohamed A. Sharaf. 2010. "Preparation of Spherical Silica Nanoparticles : Stober Silica." *Journal of American Science* 6(11):985–89.

Karimi, Mahdi, Amir Ghasemi, and Parham Sahandi Zangabad. 2016. "Smart Micro/Nanoparticles in Stimulus-Responsive Drug/Gene Delivery Systems." *Chemical Society Reviews* 45(5):1457–1501.

Kresge, C. T., M. E. Leonowicz, W. J. Roth, J. C. Vartuli, and J. S. Beck. 1992. "Ordered Mesoporous Molecular Sieves Synthesized by a Liquid-Crystal Template Mechanism." *Nature*, 359.

Kristoffersen, Arne S., Svein R. Erga, Børge Hamre, and Øyvind Frette. 2014. "Testing Fluorescence Lifetime Standards Using Two-Photon Excitation and Time-Domain Instrumentation: Rhodamine B, Coumarin 6 and Lucifer Yellow." *Journal of Fluorescence* 24(4):1015–24.

Kutcherlapati, S. N. Raj. and Rambabu Koyilapu. 2017. "Glycopolymer-Grafted Nanoparticles: Synthesis Using RAFT Polymerization and Binding Study with Lectin." *Macromolecules* 50(18):7309–20.

Li, Chunzhao and Brian C. Benicewicz. 2005. "Synthesis of Well-Defined Polymer Brushes Grafted onto Silica Nanoparticles via Surface Reversible Addition - Fragmentation Chain Transfer Polymerization." *Macromolecules* 38:5929–36.

Liu, Rui, Puhong Liao, Jikai Liu, and Pingyun Feng. 2011. “Responsive Polymer-Coated Mesoporous Silica as a PH-Sensitive Nanocarrier for Controlled Release.” *Langmuir* 3095–99.

Luís, André et al. 2015. “Synthesis , Characterization , and Biodistribution Studies of 99m Tc-Labeled SBA-16 Mesoporous Silica Nanoparticles.” *Materials Science & Engineering C* 56:181–88.

M. Rosenholm, Jessica, Cecilia Sahlgren, and Mika Linden. 2011. “Multifunctional Mesoporous Silica Nanoparticles for Combined Therapeutic, Diagnostic and Targeted Action in Cancer Treatment.” *Current Drug Targets* 12(8):1166–86.

Manzano, M., V. Aina, and C. O. Areán. 2008. “Studies on MCM-41 Mesoporous Silica for Drug Delivery : Effect of Particle Morphology and Amine Functionalization.” *Chemical Engineering Journal* 137:30–37.

Moad, Graeme, Ezio Rizzardo, and San H. Thang. 2009. “Living Radical Polymerization by the RAFT Process A Second Update.” *Australian Journal of Chemistry* 62(11):1402–72.

Mohanraj, V. J. and Y. Chen. 2006. “Nanoparticles – A Review.” *Tropical Journal of Pharmaceutical Research* 5:561–73.

Moreira, André F., Diana R. Dias, and Ilídio J. Correia. 2016. “Stimuli-Responsive Mesoporous Silica Nanoparticles for Cancer Therapy: A Review.” *Microporous and Mesoporous Materials* 236:141–57.

Nagarajan, R. 2002. “Molecular Packing Parameter and Surfactant Self-Assembly: The Neglected Role of the Surfactant Tail.” *Langmuir* 18(1):31–38.

Nakamura, Tadashi, Mamoru Mizutani, and Hiroshi Nozaki. 2007. “Formation Mechanism for Monodispersed Mesoporous Silica Spheres and Its Application to the Synthesis of Core / Shell Particles.” *Journal of Physical Chemistry* (111):1093–1100.

Neoh, Koon Gee and En Tang Kang. 2011. “Functionalization of Inorganic Nanoparticles with Polymers for Stealth Biomedical Applications.” *Polymer Chemistry* 747–59.

Patel, Vijay, Nilesh Dharaiya, and Debes Ray. 2014. “PH Controlled Size/Shape in CTAB Micelles with Solubilized Polar Additives: A Viscometry, Scattering and Spectral Evaluation.” *Colloids and Surfaces A: Physicochemical and Engineering Aspects* 455:67–75.

Popat, Amirali, Sandy Budi Hartono, and Frances Stahr. 2011. “Nanoscale and Delivery Carriers.” *Nanoscale* (3):2801–18.

Rahman, Ismail Ab and Vejayakumaran Padavettan. 2012. “Synthesis of Silica Nanoparticles by Sol-Gel : Size-Dependent Properties , Surface Modification , and Applications in Silica-Polymer Nanocomposites — A Review.” *Journal of Nanomaterials* 2012.

Ribeiro, T., E. Coutinho, A. S. Rodrigues, C. Baleizão, and J. P. S. Farinha. 2017. “Hybrid Mesoporous Silica Nanocarriers with Thermovalve-Regulated Controlled Release.” *Nanoscale* 13485–94.

Rodrigues, Ana S., Tânia Ribeiro, Fábio Fernandes, José Paulo S. Farinha, and Carlos Baleizão. 2013. “Intrinsically Fluorescent Silica Nanocontainers: A Promising Theranostic Platform.” *Microscopy and Microanalysis* 19(5):1216–21.

Rosenholm, Jessica M. and Mika Lindén. 2008. “Towards Establishing Structure-Activity Relationships for Mesoporous Silica in Drug Delivery Applications.” *Journal of Controlled Release* 128(2):157–64.

Sailor, Michael J. and Ji-ho Park. 2012. “Hybrid Nanoparticles for Detection and Treatment of Cancer.” *Advanced Materials*.

Santiago, Ana M., Carlos Baleizão, and José Paulo S. Farinha. 2015. “Multifunctional Hybrid Silica Nanoparticles with a Fluorescent Core and Active Targeting Shell for Fluorescence Imaging Biodiagnostic Applications.” *European Journal of Inorganic Chemistry* (27):4579–87.

Schmaljohann, Dirk. 2006. “Thermo- and PH-Responsive Polymers in Drug Delivery.” *Advanced Drug Delivery Reviews* 58:1655–70.

Schulz, Anja and Colette Mcdonagh. 2012. “Intracellular Sensing and Cell Diagnostics Using Fluorescent Silica Nanoparticles.” *Soft Matter* (8):2579–85.

Shakya, Akhilesh Kumar, Haider Sami, Akshay Srivastava, and Ashok Kumar. 2010. “Progress in Polymer Science Stability of Responsive Polymer – Protein Bioconjugates.” *Progress in Polymer Science* 35:459–86.

Si-Han Wu, a Chung-Yuan Moua and Hong-Ping Lin. 2013. “Synthesis of Mesoporous Silica Nanoparticles.” *Chemical Society Reviews* 42(9):3862.

Singh, Lok P., Sriman K. Bhattacharyya, and Rahul Kumar. 2014. “Sol-Gel Processing of Silica Nanoparticles and Their Applications.” *Advances in Colloid and Interface Science* 214:17–37.

Slowing, Igor, Brian G. Trewyn, and Victor S. Lin. 2006. “Effect of Surface Functionalization of MCM-41-Type Mesoporous Silica Nanoparticles on the Endocytosis by Human Cancer Cells.” *Journal of the American Chemical Society* (128):14792–93.

Stenzel, Martina H. and Thomas P. Davis. 2002. “Star Polymer Synthesis Using Trithiocarbonate Functional β-Cyclodextrin Cores (Reversible Addition-Fragmentation Chain-Transfer Polymerization).” *Journal of Polymer Science, Part A: Polymer Chemistry* 40(24):4498–4512.

Stenzel, Martina H., Thomas P. Davis, and Anthony G. Fane. 2003. “Honeycomb Structured

Porous Films Prepared from Carbohydrate Based Polymers Synthesized via the RAFT Process." *Journal of Materials Chemistry* 13(9):2090–97.

Stober, W. 1968. "Controlled Growth of Monodisperse Silica Spheres in the Micron Size Range 1." *Journal of Colloid and Interface Science* 69:62–69.

Tang, Fangqiong, Linlin Li, and Dong Chen. 2012. "Mesoporous Silica Nanoparticles: Synthesis, Biocompatibility and Drug Delivery." *Advanced Materials* 24(12):1504–34.

Trewyn, Brian G. and Hung-ting Chen. 2007. "Synthesis and Functionalization of a Mesoporous Silica Nanoparticle Based on the Sol – Gel Process and Applications in Controlled Release."

Tsujii, Yoshinobu, Muhammad Ejaz, Koichi Sato, Atsushi Goto, and Takeshi Fukuda. 2001. "Mechanism and Kinetics of RAFT-Mediated Graft Polymerization of Styrene on a Solid Surface." *Macromolecules* 8872–78.

Walker, John M. 2012. *Methods in Molecular Biology (Methods and Protocols)*.

Xing, Lei, Haoquan Zheng, Yuanyuan Cao, and Shunai Che. 2012. "Coordination Polymer Coated Mesoporous Silica Nanoparticles for PH-Responsive Drug Release." *Advanced Materials*.

Yano, Kazuhisa and Yoshiaki Fukushima. 2004. "Synthesis of Mono-Dispersed Mesoporous Silica Spheres with Highly Ordered Hexagonal Regularity Using Conventional Alkyltrimethylammonium Halide as a Surfactant." *Journal of Material Chemistry* (14):1579–84.

Yuan, Li, Qianqian Tang, and Dong Yang. 2011. "Preparation of PH-Responsive Mesoporous Silica Nanoparticles and Their Application in Controlled Drug Delivery." *The Journal of Physical Chemistry C* 115(20):9926–32.

Zauner, W., N. A. Farrow, and A. M. Haines. 2001. "In Vitro Uptake of Polystyrene Microspheres: Effect of Particle Size, Cell Line and Cell Density." *J Control Release* 71(1):39–51.

Zhou, Kejin, Yiguang Wang, and Xiaonan Huang. 2011. "Tunable, Ultrasensitive PH-Responsive Nanoparticles Targeting Specific Endocytic Organelles in Living Cells." *Angewandte Chemie - International Edition* 50(27):6109–14.

Appendix

Example of DLS result obtained for MSN4+PolyDPA. Only the samples in acidic pH meet the quality criteria.

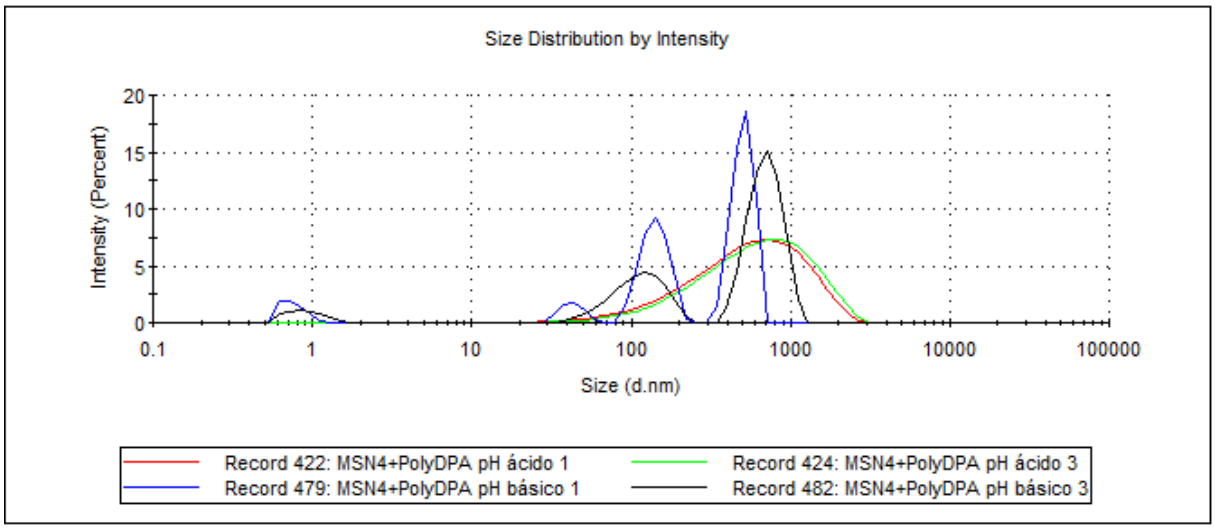

Figure 33 - Size distribution by intensity obtained by DLS for MSN4+PolyDPA in acidic pH (Red and green) and basic pH (blue and black).

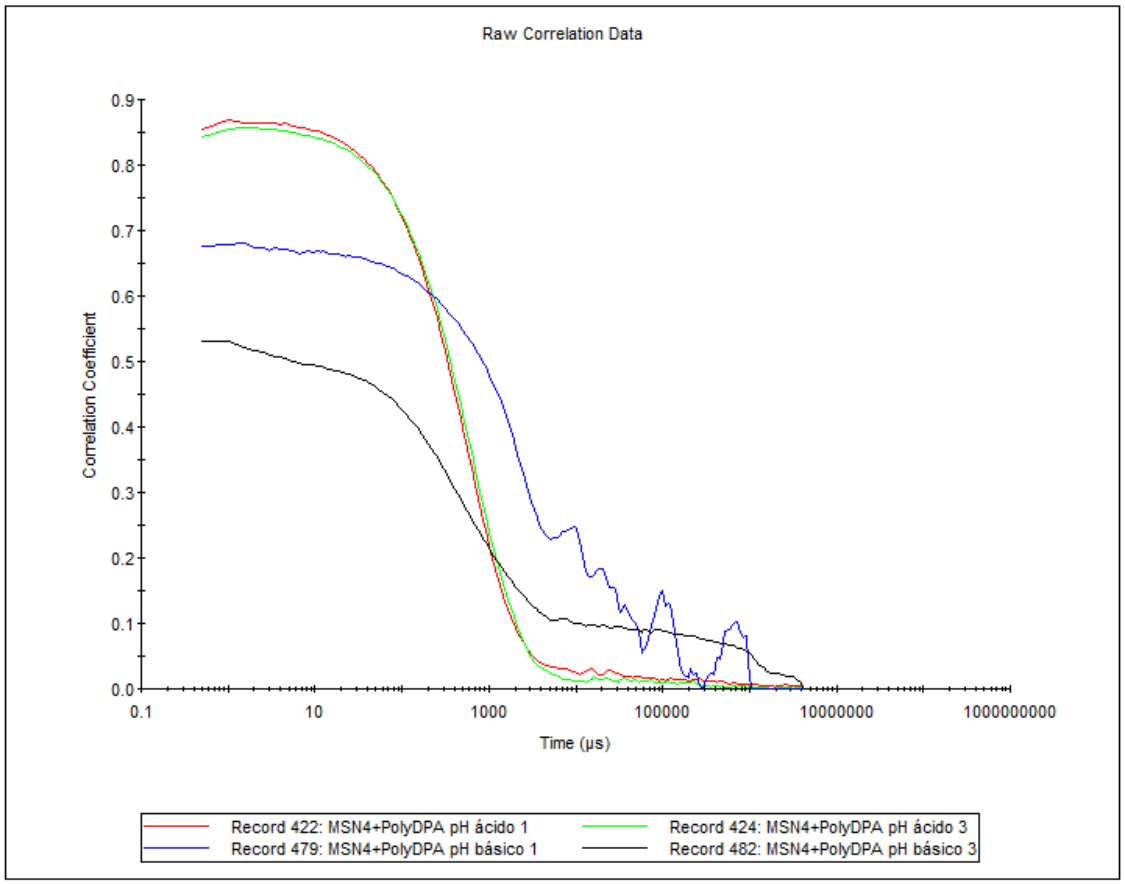

Figure 34 - Correlogram obtained by DLS for MSN4+PolyDPA in acidic pH (Red and green) and basic pH (blue and black).

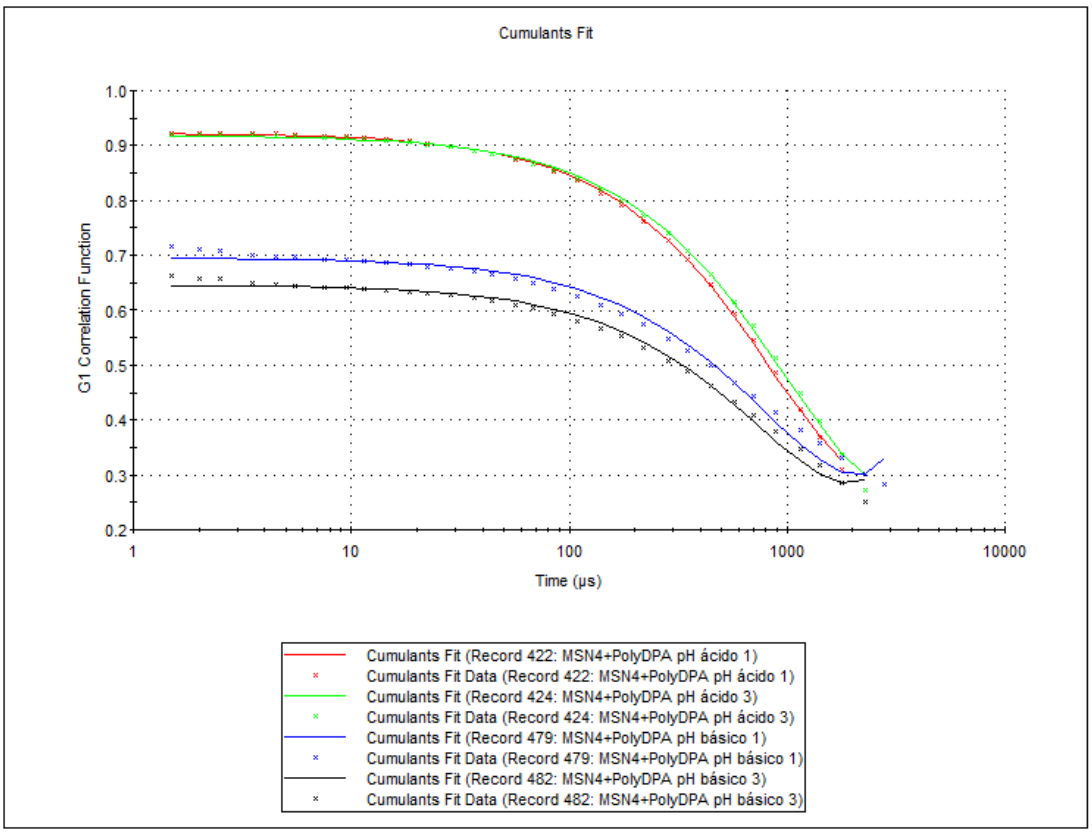

Figure 35 – Cumulant fit obtained by DLS for MSN4+PolyDPA in acidic pH (Red and green) and basic pH (blue and black).